Supporting Information
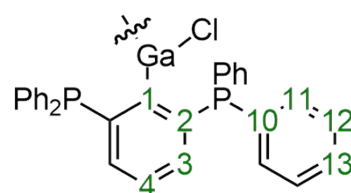
Contents

Experimental Section

General Information.

Chemicals and solvents were obtained commercially (e.g. Sigma Aldrich) and were used unchanged. Dry solvents were collected from a SPS800 MBRAUN solvent purificaton system, degassed and stored over 3 Å molecular sieves before usage. Solvents, such as 1,2-difluorobenzene (1,2-DFB), were degassed and dried directly over 3 Å molecular sieves. Deuterated solvents for NMR measurements were degased and dried directly over 3 Å molecular sieves. The corresponding ^{1}H-, ^{13}C- and ^{31}P-NMR measurements were executed (if not stated otherwise) at room temperature by using a Bruker Avance Neo 600 spectrometer. These were referenced to tetramethylsilane (^{1}H, ^{13}C) and phosphoric acid (85 % in water) (^{31}P). Chemical shifts are illustrated in parts per million (ppm). High resolution mass spectroscopy was performed with a BRUKER IMPACT II spectrometer at a flow rate of 3 μL·min^{-1}. The elemental analysis was carried out by Mikroanalytisches Laboratorium Kolbe, Oberhausen (Germany) using an Elementar Vario Micro Cube instrument.

Synthesis of R$_2$GaCl (1)

n-Butyllithium (2.40 mL, 6.00 mmol, 2.5 M in *n*-hexane 2.1 eq.) in hexane was added slowly to a solution of 1,3-bis(diphenylphosphino)-2-bromobenzene (3.00 g, 5.71 mmol, 2 eq.) in anhydrous toluene (90 mL) at room temperature and was stirred for 1.5 hours. In a separate flask GaCl$_3$ (0.503 g, 2.86 mmol, 1 eq.) was dissolved in anhydrous toluene (10 mL) and cooled to –78 °C. The lithium organyl was added within 20 minutes to the GaCl$_3$ solution at –78 °C. The reaction mixture was allowed to warm up to room temperature overnight while stirring. The reaction mixture was filtered under argon atmosphere over Celite and the solvent

was removed under vacuum. The residue was washed with dry *n*-hexane (2 × 25 mL) and dried under vacuum. The product was obtained as a colorless solid (2.7 g, 2.71 mmol, 94.78%). Suitable single crystals for X-ray structure determinations were obtained by recrystallization from toluene/*n*-hexane.

^{1}H-NMR (600 MHz, THF-d8): δ = 7.38 (d, 4H, H_3), 7.27 (t, 2H, H_4), 7.20-7.16 (m, 24H, H_{12}+H_{13}), 7.11 (t, 16H, H_{11}) ppm. **^{13}C{^{1}H}-NMR (150.9 MHz, THF-d8):** δ = 172.84 (m, C_1), 144.3 (s, C_2), 138.2 (s, C_{10}), 136.6 (s, C_3), 134.2 (m, C_{12}), 130.6 (s, C_4), 129.2 (s, C_{13}), 129.1 (s, C_{11}) ppm. **^{31}P-NMR (243 MHz, THF-d8):** δ = –3.02 (s) ppm. **Anal. Calcd.** for $C_{60}H_{46}ClGaP_4$ [%]: C, 72.35; H, 4.66; Found: C, 72.41; H, 4.63; **Mp**: 229 °C.

Synthesis of [R$_2$-Ni$_2$Cl][GaCl$_4$] (2Ni)

Dry 1,2-difluorobenzene (8 mL) was added to Ni(dme)Cl$_2$ (66.17 mg, 0.30 mmol, 2 eq.) and R$_2$GaCl (150 mg, 0.15 mmol, 1 eq.). The reaction mixture was stirred for 24 hours at 60 °C. The solvent was removed under vacuum. The residue was

dissolved in anhydrous DCM and filtered via a syringe filter to remove the dimethoxyethane from the desired product. The solvent was removed under vacuum. The residue was recrystallized from DCM/*n*-hexane to obtain [R$_2$-Ni$_2$Cl][GaCl$_4$] (143.88 mg, 0.138 mmol, 91.54 %) as a red powder. The product is sensitive to solvents such as MeCN or CHCl$_3$, oxygen and moisture, but is storable under inert conditions for several weeks. Suitable single crystals for X-ray structure determinations were obtained by recrystallization from THF/*n*-hexane.
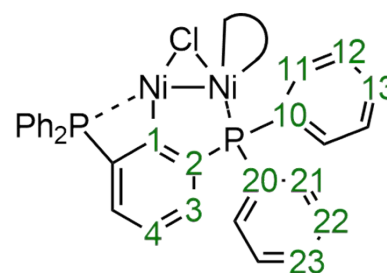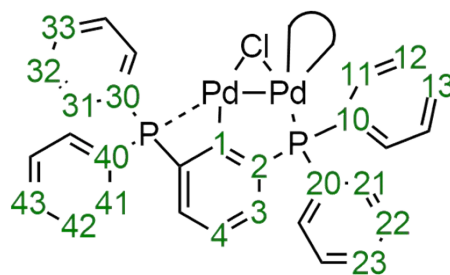
^{1}H-NMR (600 MHz, CD$_2$Cl$_2$): δ = 7.79 (dd, $^3J(^{31}P-^1H)$ = 13.3 Hz, $^3J(^1H-^1H)$ = 7.6 Hz, 4H, H_{21}), 7.69 – 7.63 (m, 4H, H_{23}+(PPh$_2$)$_c$-H$_{Aryl}$), 7.51 – 7.48 (m, 4H, H_{22}), 7.47 – 7.41 (m, 10H, (PPh$_2$)$_c$-H$_{aryl}$), 7.36 (t, $^3J(^1H-^1H)$ = 7.5 Hz, 6H, H_3+(PPh$_2$)$_c$-H$_{aryl}$), 7.32 (d, $^3J(^1H-^1H)$ = 7.7 Hz,

2H, (PPh$_2$)$_c$-H$_{aryl}$), 7.25 (t, $^3J(^1$H-^{1}H) = 7.5 Hz, 2H, H$_{13}$), 7.20 (dd, $^3J(^1$H-^{1}H) = 12.9 Hz, $^5J(^1$H-^{1}H) = 7.7 Hz, 4H, (PPh$_2$)$_c$-H$_{aryl}$), 7.05 (m, 2H, H$_4$), 6.93 (t, $^3J(^1$H-^{1}H) = 6.8 Hz, 4H, H$_{12}$), 6.73 (dd, $^3J(^{31}$P -^{1}H) = 10.2 Hz, $^3J(^1$H-^{1}H) = 7.8 Hz, 4H, H$_{11}$) ppm. **^{13}C{^{1}H}-NMR (150.9 MHz, CD$_2$Cl$_2$):** δ = 153.0 (ddd, $^1J(^{31}$P-^{13}C) = 93.6 Hz, $^3J(^{31}$P-^{13}C) = 61.4 Hz, $^3J(^{31}$P-^{13}C) = 31.7 Hz, C$_2$), 146.2 (dd, $^2J(^{31}$P-^{13}C) = 55.3, $^2J(^{31}$P-^{13}C) = 22.5 Hz, C$_1$), 141.4 (d, $^1J(^{31}$P-^{13}C) = 44.4 Hz, C$_{10}$), 138.8 (s, C$_4$), 134.0 (d, $J(^{31}$P-^{13}C) = 14.3 Hz, (PPh$_2$)$_c$-C$_{aryl}$), 133.9 (d, $^2J(^{31}$P-^{13}C) = 12.0 Hz, C$_{21}$), 132.9 (d, $^2J(^{31}$P-^{13}C) = 10.6 Hz, C$_{11}$), 132.8 (s, (PPh$_2$)$_c$-C$_{aryl}$), 132.7 (s, C$_{23}$), 131.5 (s, (PPh$_2$)$_c$-C$_{aryl}$), 130.8 (s, C$_{13}$), 130.2 (s, (PPh$_2$)$_c$-C$_{aryl}$), 130.2 (s, (PPh$_2$)$_c$-C$_{aryl}$), 130.0 (d, $^3J(^{31}$P-^{13}C) = 11.5 Hz, C$_{22}$), 129.5 (d, ^2J = 10.4 Hz, C$_3$), 129.0 (d, ^3J (^{31}P-^{13}C) = 9.1 Hz, C$_{12}$), 128.3 (d, ^1J (^{31}P-^{13}C) = 44.5 Hz, C$_{20}$), 126.7 (d, ^1J = 43.5 Hz, (PPh$_2$)$_c$-C$_q$) ppm. **^{31}P-NMR (243 MHz, CD$_2$Cl$_2$):** δ = 9.16 (m), –60.48 (m) ppm. **Mp**: Decomposition at 207 °C. **HRMS (ESI, positive mode, DCM/MeCN 1:10):** m/z 1041.09374 [M–[GaCl$_4$]]$^+$, Err. 0.25 mDa, m/z 503.06.06229 [M-Cl]$^{2+}$, Err. –0.01 mDa.

Synthesis of [R$_2$Pd$_2$Cl][GaCl$_4$] (2Pd)

PdCl$_2$ (53.40 mg, 0.30 mmol, 2 eq.) was refluxed in anhydrous MeCN (3 mL) for 45 min. The solvent was removed under vacuum to obtain Pd(MeCN)$_2$Cl$_2$ as a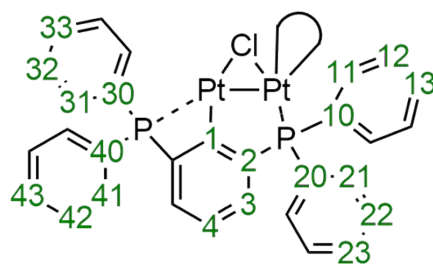n orange solid. R$_2$GaCl (150 mg, 0.15 mmol, 1 eq.) and anhydrous 1,2-difluorobenzene (8 mL) was added and the reaction mixture was stirred for 24 hours at 45 °C. The solvent was removed under reduced pressure. For purification a stepwise recrystallization from THF/toluene was performed to obtain [R$_2$Pd$_2$Cl][GaCl$_4$] (122.88 mg, 0.11 mmol, 71.63 %) as a orange powder. The product can be stored in air for several months without any decomposition. Suitable single crystals for X-ray structure determinations were obtained by recrystallization from acetone/n-pentane.

¹H-NMR (600 MHz, CD₂Cl₂): δ = 7.65 (m, 2H, H_{23}) 7.64 (d, $^3J(^1H\text{-}^1H)$ = 7.6 Hz, 2H, H_{33}), 7.60 – 7.55 (m, 4H, H_{42}), 7.50 (t, $^3J(^1H\text{ -}^1H)$ = 7.4 Hz, 4H, H_{41}), 7.47 – 7.43 (m, 14H, $H_{21}+H_{22}+H_{32}+H_{43}$), 7.42 – 7.38 (m, 4H, H_3), 7.34 – 7.31 (m, 4H, H_{31}), 7.30 (d, $^3J(^1H\text{-}^1H)$ = 6.6 Hz, 2H, H_{13}), 7.22 (m, 2H, H_4), 7.01 (t, $^3J(^1H\text{ -}^1H)$ = 7.6 Hz, 4H, H_{12}), 6.83 (dd, $^3J(^{31}P\text{-}^1H)$ = 10.4, $^3J(^1H\text{-}^1H)$ = 7.1 Hz, 4H, H_{11}) ppm. **¹³C{¹H}-NMR (150.9 MHz, CD₂Cl₂):** δ = 153.0 (dt, $^1J(^{31}P\text{-}^{13}C)$ = 149.4 Hz, $^3J(^{31}P\text{-}^{13}C)$ = 25.3 Hz, C_2), 147.7 (dt, $^2J(^{31}P\text{-}^{13}C)$ = 56.1 Hz, $^2J(^{31}P\text{-}^{13}C)$ = 9.8 Hz, C_1), 139.7 (dd, $^1J(^{31}P\text{-}^{13}C)$ = 50.9 Hz, $^5J(^{31}P\text{-}^{13}C)$ = 5.2 Hz, C_{40}), 139.4 (t, $^3J(^{31}P\text{-}^{13}C)$ = 5.0 Hz, C_4), 134.6 (m, C_{42}), 134.1 (dd, $^1J(^{31}P\text{-}^{13}C)$ = 36.3 Hz, $^5J(^{31}P\text{-}^{13}C)$ = 3.0 Hz, C_{10}), 133.8 (d, $^2J(^{31}P\text{-}^{13}C)$ = 12.8 Hz, C_{21}), 133.1 (s, C_{31}), 133.0 (s, C_{33}), 132.8 (d, $^4J(^{31}P\text{-}^{13}C)$ = 2.9 Hz, C_{23}), 132.6 (m, C_{11}), 131.9 (m, C_{32}), 131.6 (s, C_{41}), 130.9 (s, C_{13}), 130.3 (d, $^3J(^{31}P\text{-}^{13}C)$ = 12.3 Hz, C_{22}), 130.0 (d, $^3J(^{31}P\text{-}^{13}C)$ = 12.6 Hz, C_{22}) 129.5 (d, $^4J(^{31}P\text{-}^{13}C)$ = 5.3 Hz, C_{43}), 129.5 (s, C_3), 129.3 (m, C_{12}), 128.7 (d, $^1J(^{31}P\text{-}^{13}C)$ = 51.1 Hz, C_{20}), 126.7 (dt, $^1J(^{31}P\text{-}^{13}C)$ = 50.7 Hz, $^5J(^{31}P\text{-}^{13}C)$ = 1.5 Hz, C_{30}) ppm. **³¹P-NMR (243 MHz, CD₂Cl₂):** δ = 8.2 (t, $^2J(^{31}P\text{-}^{31}P)$ = 5.1 Hz), –76.3 (t, $^2J(^{31}P\text{-}^{31}P)$ = 5.1 Hz) ppm. **Mp**: Decomposition at 238 °C. **HRMS (ESI, positive mode, DCM/MeCN 1:10):** m/z 1137.03158 [M–[GaCl₄]]⁺, Err. 1.06 mDa.

Synthesis of [R₂Pt₂Cl][GaCl₄] (2Pt)

Dry THF (8 mL) was added to R₂GaCl (100 mg, 0.10 mmol, 1 eq.) and Pt(MeCN)₂Cl₂ (69.89 mg, 0.20 mmol, 2 eq.) and was stirred for 5 days at 50 °C. The reaction mixture was filtered and for purification the THF phase was layered with *n*-hexane in a 1:1 ratio. The precipitate was washed with *n*-hexane (2 × 5 mL) to obtain [R₂Pt₂Cl][GaCl₄] (84.34 g, 0.064 mmol, 63.81 %) as a red solid. The product is stable in air for several weeks without decomposition. Suitable single crystals for X-ray structure determinations were obtained by recrystallization from THF/*n*-hexane.

^{1}H-NMR (600 MHz, CD$_2$Cl$_2$): δ = 7.66 – 7.63 (m, 4H, H$_{31}$), 7.62 – 7.60 (m, 4H, H$_{21}$), 7.50 (td, $^3J(^1\text{H-}^1\text{H})$ = 7.3 Hz, $^4J(^1\text{H-}^1\text{H})$ = 1.6 Hz, 2H, H$_{23}$), 7.46 – 7.42 (m, 12H, H$_{22}$, H$_{32}$, H$_{41}$), 7.42 – 7.39 (m, 4H, H$_{42}$), 7.37 (dd, $^3J(^1\text{H-}^1\text{H})$ = 7.7 Hz, $^4J(^{31}\text{P-}^1\text{H})$ = 3.6 Hz, 2H, H$_4$), 7.32 (dd, $^3J(^1\text{H-}^1\text{H})$ = 12.1 Hz, $^4J(^1\text{H-}^1\text{H})$ = 8.3 Hz, 2H, H$_{43}$), 7.28 (d, $^3J(^1\text{H-}^1\text{H})$ = 8.3 Hz, 2H, H$_{13}$) 7.25 (d, $^3J(^1\text{H-}^1\text{H})$ = 8.3 Hz, 4H, H$_3$), 7.24 (d, $^3J(^1\text{H-}^1\text{H})$ = 7.1 Hz, 2H, H$_{33}$), 6.97 (td, $^3J(^1\text{H-}^1\text{H})$ = 7.9 Hz, $^4J(^1\text{H-}^1\text{H})$ = 2.1 Hz, 4H, H$_{12}$), 6.78 (ddd, $^3J(^{31}\text{P-}^1\text{H})$ = 11.4 Hz, $^3J(^1\text{H-}^1\text{H})$ = 8.2 Hz, $^4J(^1\text{H-}^1\text{H})$ = 1.4 Hz, 4H, H$_{11}$) ppm. **^{13}C{^{1}H}-NMR (150.9 MHz, CD$_2$Cl$_2$):** δ = 151.2 (dd, $^1J(^{31}\text{P-}^{13}\text{C})$ = 65.4 Hz, $^3J(^{31}\text{P-}^{13}\text{C})$ = 16.9 Hz, C$_2$), 149.2 (dt, $^2J(^{31}\text{P-}^{13}\text{C})$ = 125.5 Hz, $^2J(^{31}\text{P-}^{13}\text{C})$ = 23.4 Hz, C$_1$), 139.2 (s, C$_3$), 134.8 (d, $^2J(^{31}\text{P-}^{13}\text{C})$ = 12.3 Hz, C$_{21}$), 134.1 (d, $^1J(^{31}\text{P-}^{13}\text{C})$ = 47.7 Hz, C$_{10}$), 133.8 (s, C$_{42}$), 133.7 (s, C$_{32}$), 133.1 (s, C$_{41}$), 132.7 (d, $^2J(^{31}\text{P-}^{13}\text{C})$ = 7.0 Hz, C$_{11}$), 132.7 (d, $^4J(^{31}\text{P-}^{13}\text{C})$ = 7.2 Hz, C$_{43}$), 131.8 (s, C$_{33}$), 131.8 (s, C$_{23}$), 131.2 (s, C$_{13}$), 130.2 (d, $^1J(^{31}\text{P-}^{13}\text{C})$ = 12.1 Hz, C$_{30}$), 129.8 (d, $^4J(^{31}\text{P-}^{13}\text{C})$ = 12.5 Hz, C$_{22}$) 129.6 (d, $^2J(^{31}\text{P-}^{13}\text{C})$ = 10.9 Hz, C$_{31}$), 129.1 (d, $^3J(^{31}\text{P-}^{13}\text{C})$ = 9.8 Hz, C$_{12}$), 128.6 (dd, $^3J(^{31}\text{P-}^{13}\text{C})$ = 12.7 Hz, $^3J(^{31}\text{P-}^{13}\text{C})$ = 4.1 Hz, C$_4$), 126.9 (d, $^1J(^{31}\text{P-}^{13}\text{C})$ = 59.6 Hz, C$_{40}$), 126.3 (d, $^1J(^{31}\text{P-}^{13}\text{C})$ = 61.6 Hz, C$_{20}$) ppm. **^{31}P-NMR (243 MHz, CD$_2$Cl$_2$):** δ = 13.0 (s, $^1J(^{123}\text{Pt-}^{31}\text{P})$ = 2072.6 Hz), –76.1 (s, $^1J(^{123}\text{Pt-}^{31}\text{P})$ = 4081.2 Hz) ppm. **Mp**: > 300 °C. **HRMS (ESI, positive mode, DCM/MeCN 1:10):** m/z 1315.15093 [M–[GaCl$_4$]]$^+$, Err. 1.25 mDa.

Synthesis of R$_2$GaCl-(PtCl$_2$) (1·PtCl$_2$)

Dry 1,2-difluorobenzene (2 mL) was added to R$_2$GaCl (50 mg, 0.05 mmol, 1 eq.) and Pt(Et$_2$S)$_2$Cl$_2$ (22.41 mg, 0.05 mmol, 1 eq.) and was stirred for 4 days at room temperature. The desired product precipitates as a yellow solid. The reaction solvent was decanted off and the precipitate was washed with n-hexane (3 × 4 mL) and cold 1,2-difluorobenzene (2 × 2 mL) to obtain R$_2$GaCl-(PtCl$_2$) (37.62 g, 0.03 mmol, 59.39 %) as a yellow solid. The product is stable

in air for several weeks without decomposition. Suitable single crystals for X-ray structure determinations were obtained by recrystallization from DCM/*n*-hexane.

^{1}H-NMR (600 MHz, CD$_2$Cl$_2$, 243 K): δ = 8.06 (dd, $J(^{31}P\text{-}^1H)$ = 11.7 Hz, $J(^1H\text{-}^1H)$ = 7.5 Hz, 2H), 7.60 (d, $J(^1H\text{-}^1H)$ = 7.7 Hz, 2H), 7.52 (td, $J(^1H\text{-}^1H)$ = 8.2 Hz, $J(^1H\text{-}^1H)$ = 2.9 Hz, 2H), 7.48 – 7.21 (m, 25H), 7.20 – 7.15 (m, 4H), 7.12 (t, $J(^1H\text{-}^1H)$ = 7.9 Hz, 4H), 7.04 (td, $J(^1H\text{-}^1H)$ = 7.3 Hz, $J(^1H\text{-}^1H)$ = 2.3 Hz, 1H), 6.90 (dd, $J(^{31}P\text{-}^1H)$ = 12.4 Hz, $J(^1H\text{-}^1H)$ = 7.9 Hz, 2H), 6.78 (t, $J(^1H\text{-}^1H)$ = 7.5 Hz, 1H), 6.21 (t, $J(^1H\text{-}^1H)$ = 7.9 Hz, 2H), 6.11 (s$_{(br)}$, 1H) ppm. **^{13}C{^{1}H}-NMR (150.9 MHz, CD$_2$Cl$_2$, 243 K):** δ = 173.4 (dd, $J(^{31}P\text{-}^{13}C)$ = 99.4 Hz, $J(^{31}P\text{-}^{13}C)$ = 38.0 Hz, C$_2$), 166.1 (ddd, $J(^{31}P\text{-}^{13}C)$ = 54.0 Hz, $J(^{31}P\text{-}^{13}C)$ = 36.2 Hz, $J(^{31}P\text{-}^{13}C)$ = 8.1 Hz, C$_1$), 145.5 (ddd, $J(^{31}P\text{-}^{13}C)$ = 20.5 Hz, $J(^{31}P\text{-}^{13}C)$ = 12.9 Hz, $J(^{31}P\text{-}^{13}C)$ = 2.5 Hz, C$_q$), 143.5 (td, $J(^{31}P\text{-}^{13}C)$ = 19.0 Hz, $J(^{31}P\text{-}^{13}C)$ = 3.2 Hz, C$_q$), 139.6 (dd, $J(^{31}P\text{-}^{13}C)$ = 15.2 Hz, $J(^{31}P\text{-}^{13}C)$ = 5.1 Hz), 138.4 (s), 137.7 (d, $J(^{31}P\text{-}^{13}C)$ = 15.1 Hz, C$_q$), 137.1 (dd, $^1J(^{31}P\text{-}^{13}C)$ = 74.2 Hz, $J(^{31}P\text{-}^{13}C)$ = 16.9 Hz, C$_q$), 135.4 (s), 134.6 (s), 134.5 (d, $J(^{31}P\text{-}^{13}C)$ = 7.9 Hz), 134.0 (s), 133.9 (s), 133.6 (d, $J(^{31}P\text{-}^{13}C)$ = 18.3 Hz), 133.5 (d, $J(^{31}P\text{-}^{13}C)$ = 4.3 Hz), 133.4 (d, $J(^{31}P\text{-}^{13}C)$ = 13.8 Hz), 133.2 (d, $J(^{31}P\text{-}^{13}C)$ = 15.6 Hz), 133.1 (s), 133.0 (d, $J(^{31}P\text{-}^{13}C)$ = 17.9 Hz), 132.5 (s), 131.7 (d, $J(^{31}P\text{-}^{13}C)$ = 69.5 Hz, C$_q$), 131.0 (d, $J(^{31}P\text{-}^{13}C)$ = 8.7 Hz), 130.6 (d, $J(^{31}P\text{-}^{13}C)$ = 27.5 Hz), 130.4 (d, $J(^{31}P\text{-}^{13}C)$ = 7.2 Hz), 129.8 (d, $J(^{31}P\text{-}^{13}C)$ = 29.6 Hz), 129.1 (d, $J(^{31}P\text{-}^{13}C)$ = 11.6 Hz), 129.0 (d, $J(^{31}P\text{-}^{13}C)$ = 8.1 Hz), 128.8 (d, $J(^{31}P\text{-}^{13}C)$ = 7.3 Hz), 128.5 (s), 128.4 (s), 128.4 (s), 128.1 (d, $J(^{31}P\text{-}^{13}C)$ = 36.1 Hz), 127.2 (dd, $J(^{31}P\text{-}^{13}C)$ = 30.7 Hz, $J(^{31}P\text{-}^{13}C)$ = 11.1 Hz), 126.9 (d, $^1J(^{31}P\text{-}^{13}C)$ = 64.0 Hz, C$_q$), 126.5 (d, $^1J(^{31}P\text{-}^{13}C)$ = 60.2 Hz, C$_q$) ppm. **^{31}P-NMR (243 MHz, CD$_2$Cl$_2$, 243 K):** δ = 30.1 (s, $^1J(^{195}Pt\text{-}^{31}P)$ = 3430 Hz), 24.7 ($^1J(^{195}Pt\text{-}^{31}P)$ = 3016 Hz), –1.7 (d, $^4J(^{31}P\text{-}^{31}P)$ = 101.9 Hz), –10.1 (d, $^4J(^{31}P\text{-}^{31}P)$ = 102 Hz) ppm. **Mp**: Decomposition at 271 °C. **HRMS (ESI, positive mode, DCM/MeCN 1:10):** *m/z* 1227.08229 [M-Cl]$^+$, Err. –0.8 mDa.

Catalysis of Me₂NH-BH₃ by using 2·Ni / 2·Pt

Catalysis experiments were performed by using the "gas evolution measurement device Man on the Moon (Series 104)". First of all a blank experiment was performed to obtain data for the heating process. The measurement was stopped after around 50 minutes due to constant pressure. Therefore 0.7 mL 1,2-difluorobenzene and $Me_2NH\text{-}BH_3$ (6.05 mg, 25 eq.) were submitted into the suitable flask which is connected to the gas evolution measurement device Man on the Moon (Series 104). For further measurements 4.30 mg **2Ni** (4.12 μmol, 4 Mol-%) or 5.40 mg **2Pt** (4.10 μmol, 4 Mol-%) and 6.05 mg $Me_2NH\text{-}BH_3$ (4.12 μmol, 25 eq.) were used. The reaction mixture wase dissolved in dry and degassed 1,2-difluorobenzene (0.7 mL). To start the experiment the reaction flask was transferred into an oil bath at 70 °C and simultaneously the measurement was started by using the Man on the Moon X104 software. According to the ideal gas law the pressure generated within the reactions was expected to be at 218 mbar. Data was collected until 50 minutes, with three data points per second, of reaction and was stopped afterwards due to almost constant linear progress of data points. To investigate the catalysis via NMR spectroscopy identical reaction scales were transferred to a J-Young NMR tube and were placed into oil bath at 70 °C.
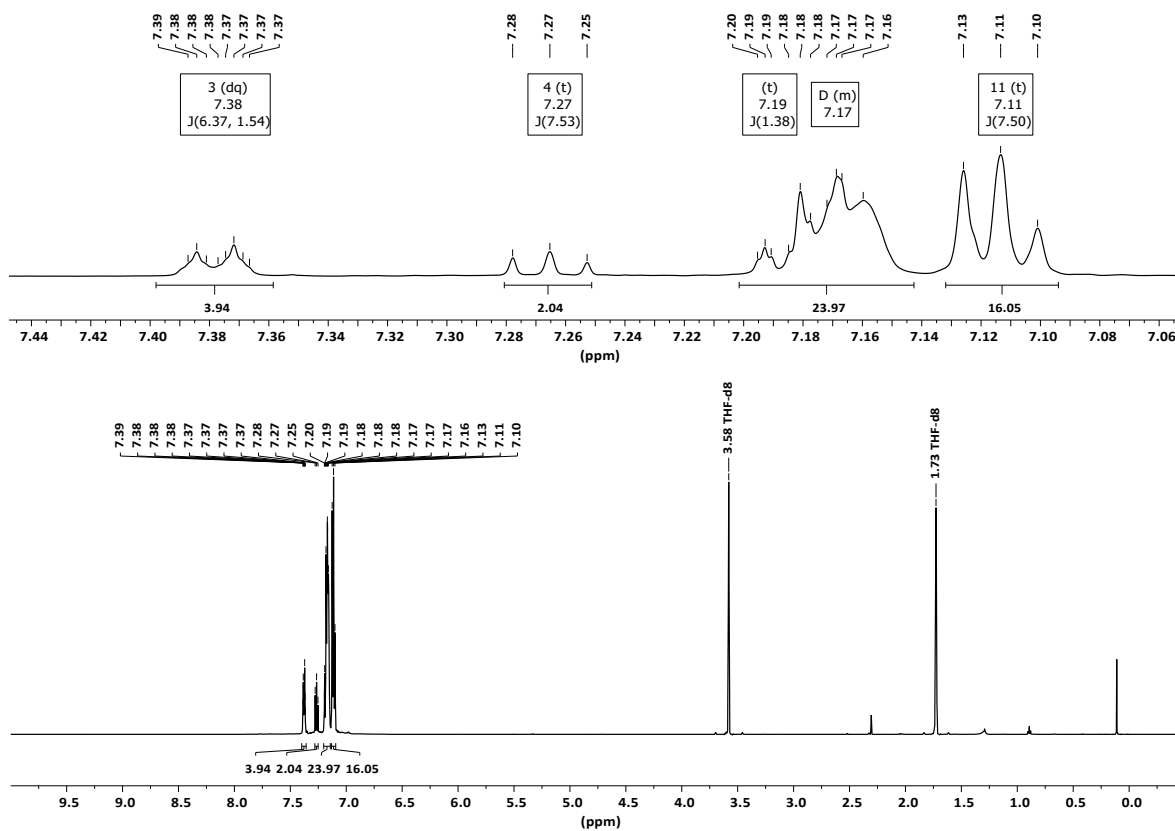
NMR Spectra

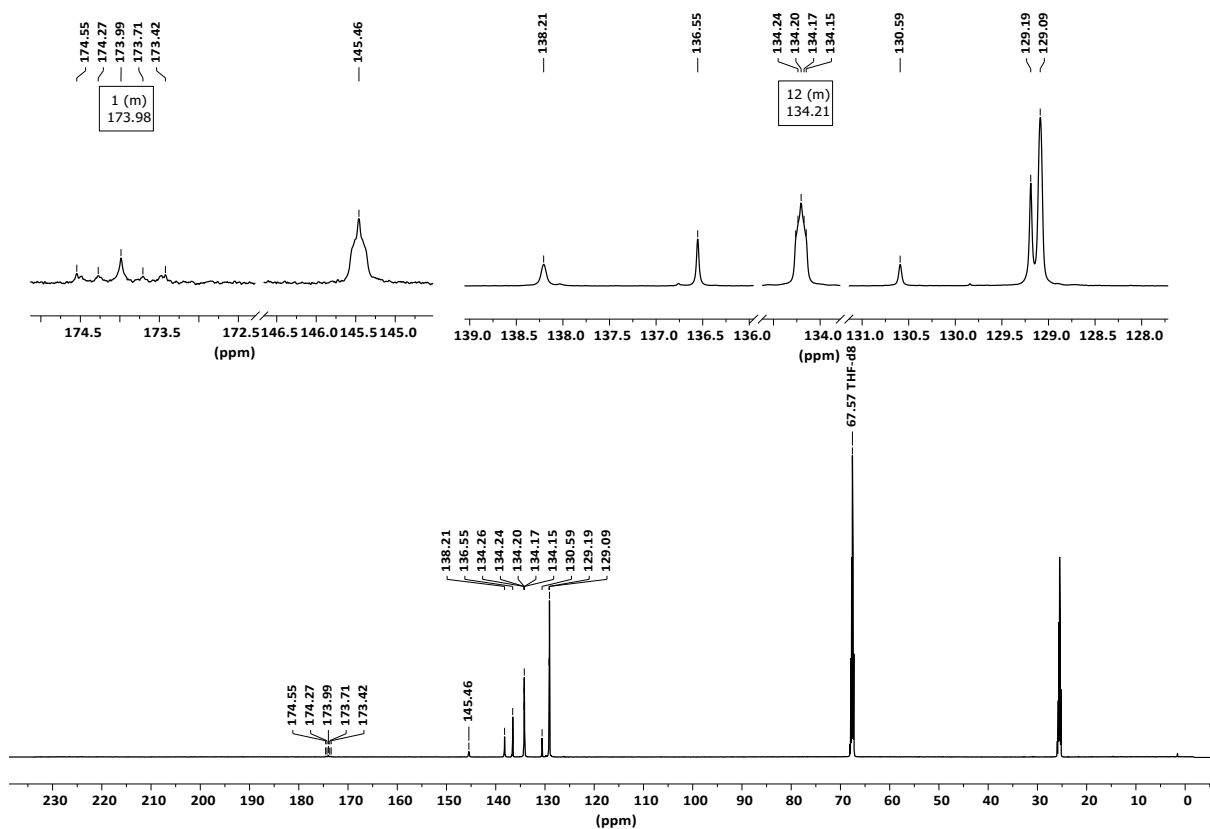**Figure S1a**: ^{1}H NMR spectrum (THF-d8, 600 MHz) of **1.**

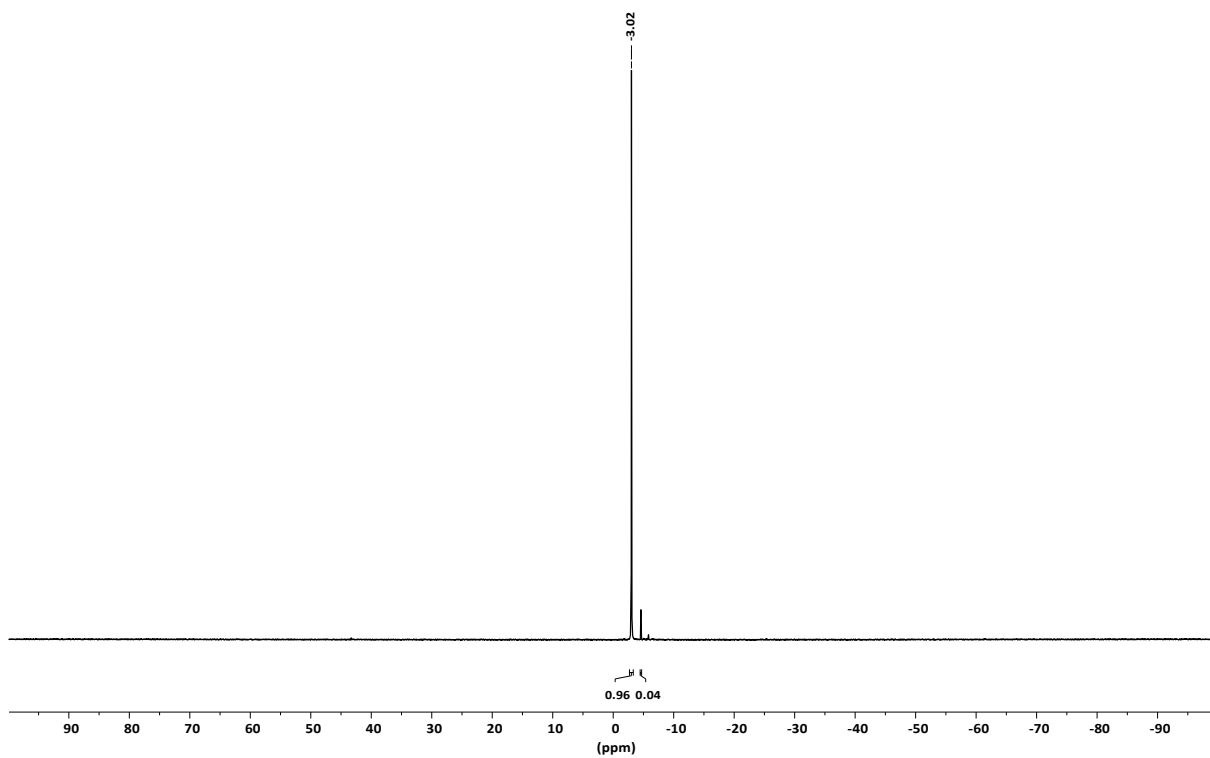**Figure S1b**: $^{13}C\{^1H\}$ NMR spectrum (THF-d8, 151 MHz) of **1**.

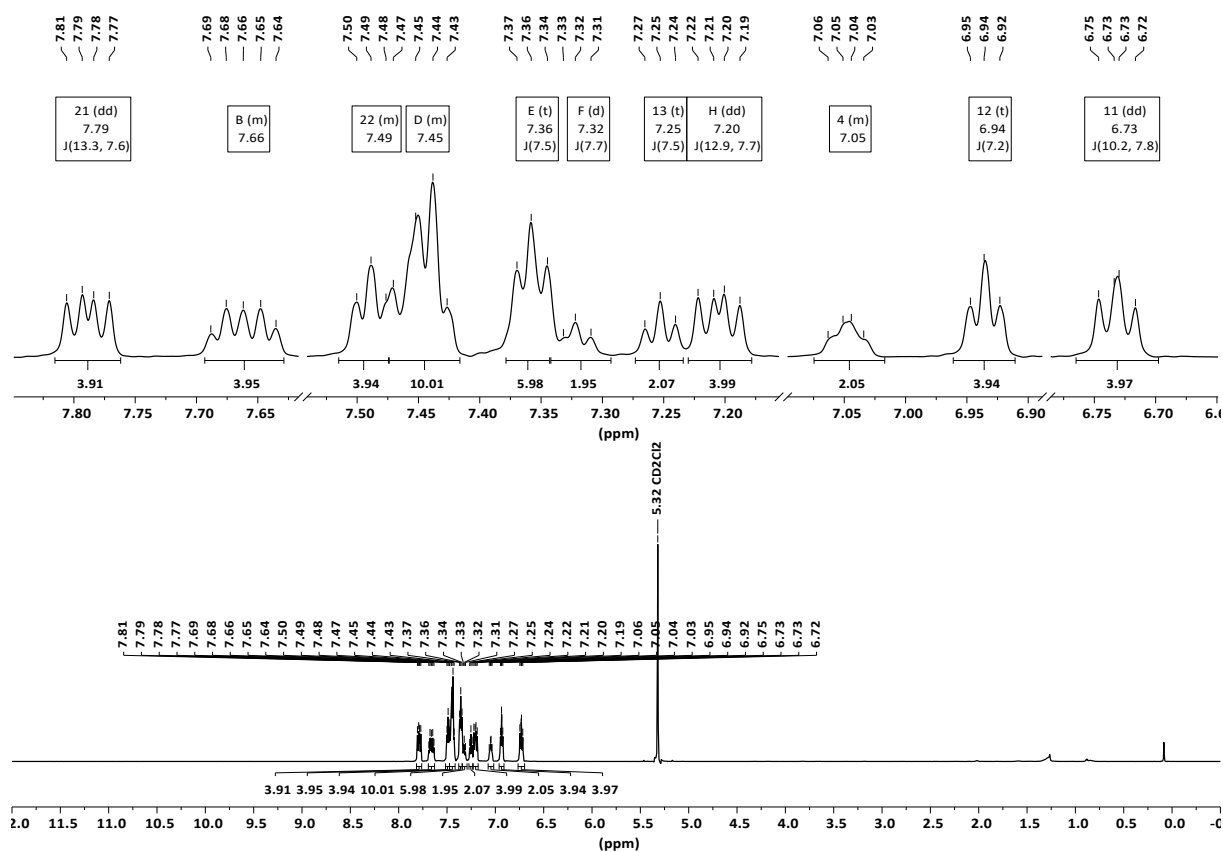**Figure S1c**: ^{31}P NMR spectrum (THF-d8, 151 MHz) of **1**.

10

Figure S2a: ^1H NMR spectrum (CD$_2$Cl$_2$, 600 MHz) of **2Ni**.
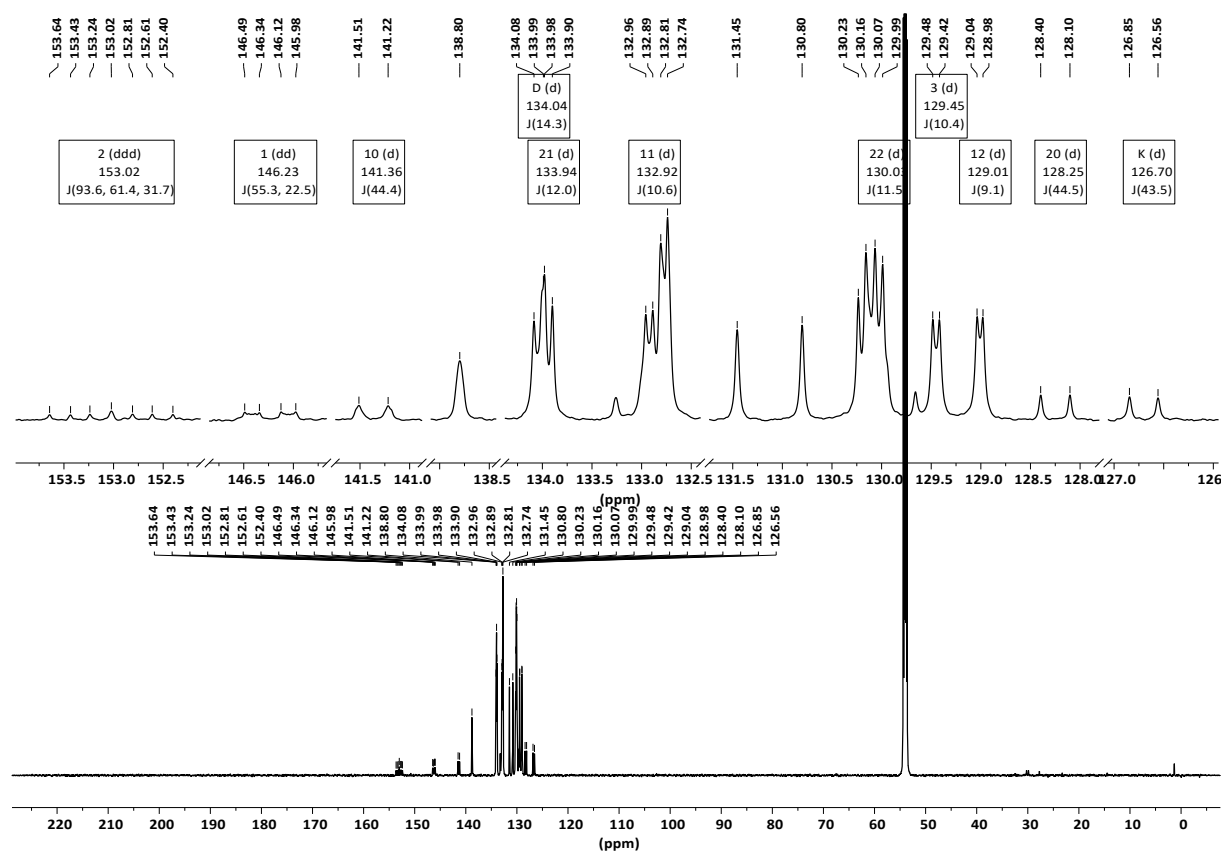
Figure S2b: $^{13}C\{^1H\}$ NMR spectrum (CD$_2$Cl$_2$, 600 MHz) of **2Ni**.

11
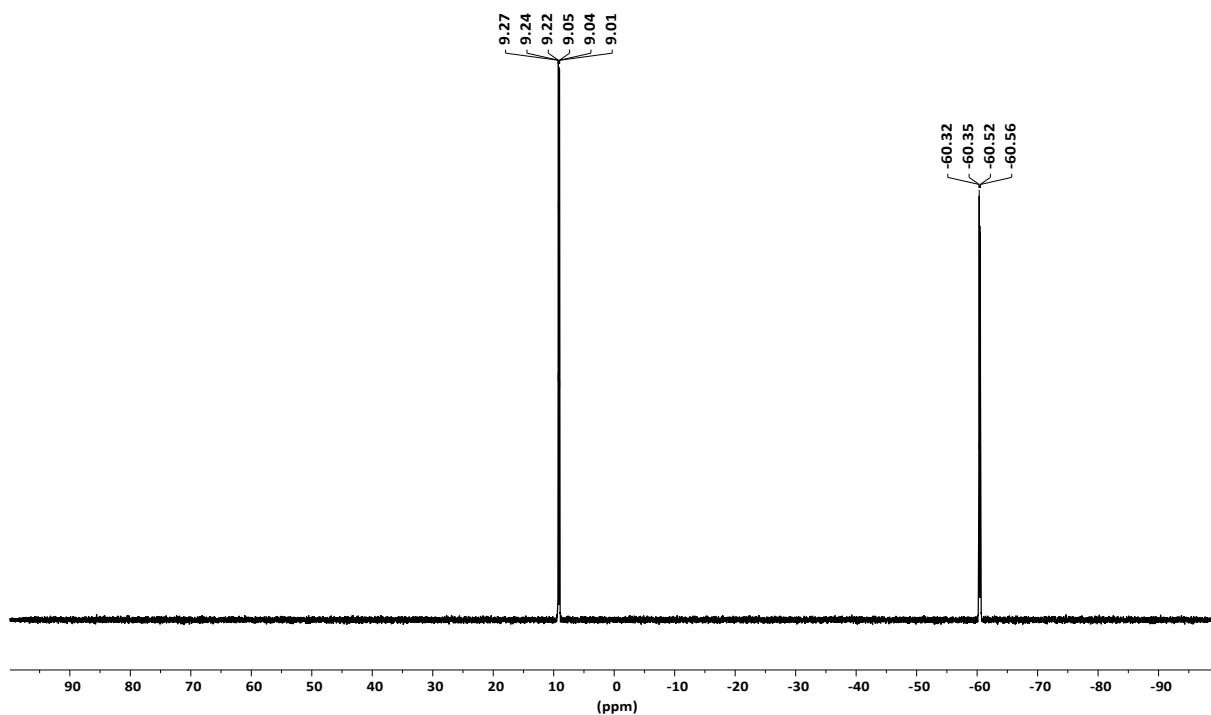
Figure S2c: ^{31}P NMR spectrum (CD$_2$Cl$_2$, 243 MHz) of **2Ni**.
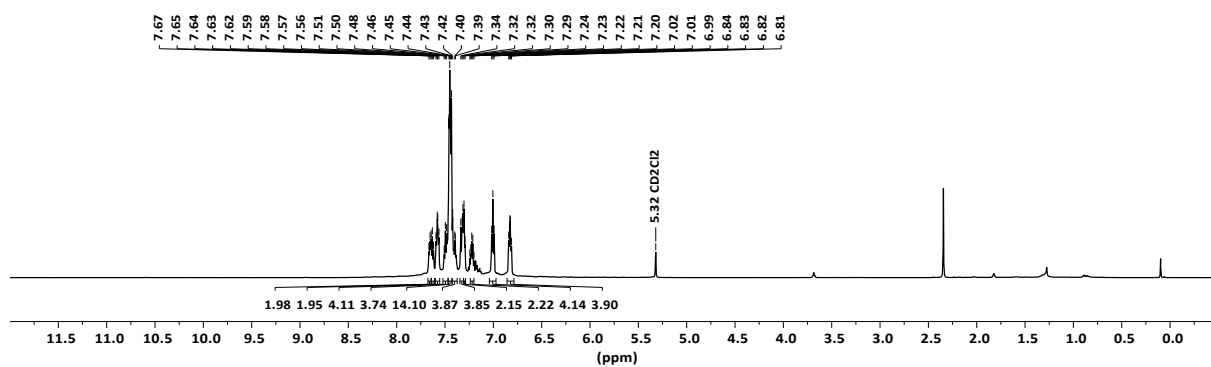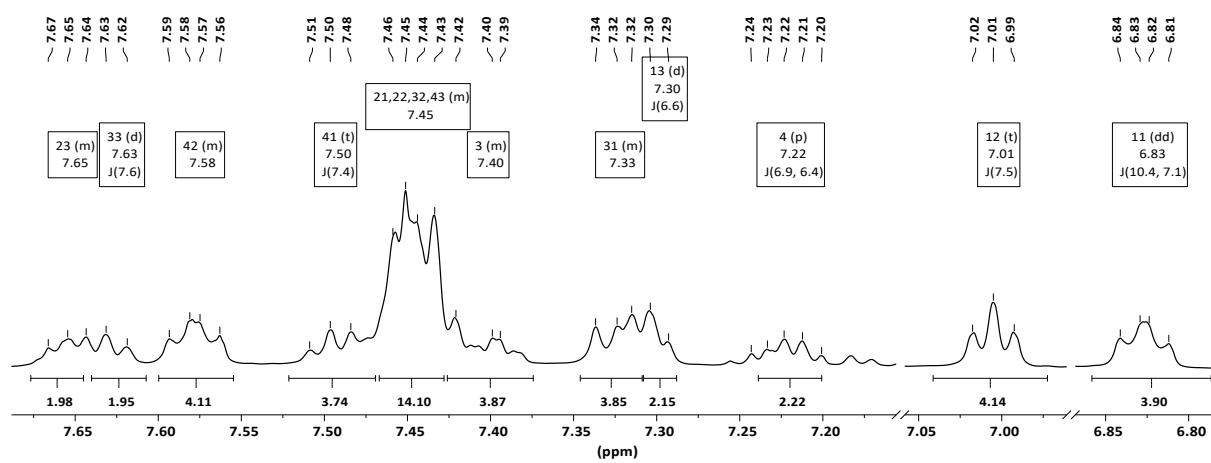
Figure S3a: ^1H NMR spectrum (CD$_2$Cl$_2$, 600 MHz) of **2Pd**.

12
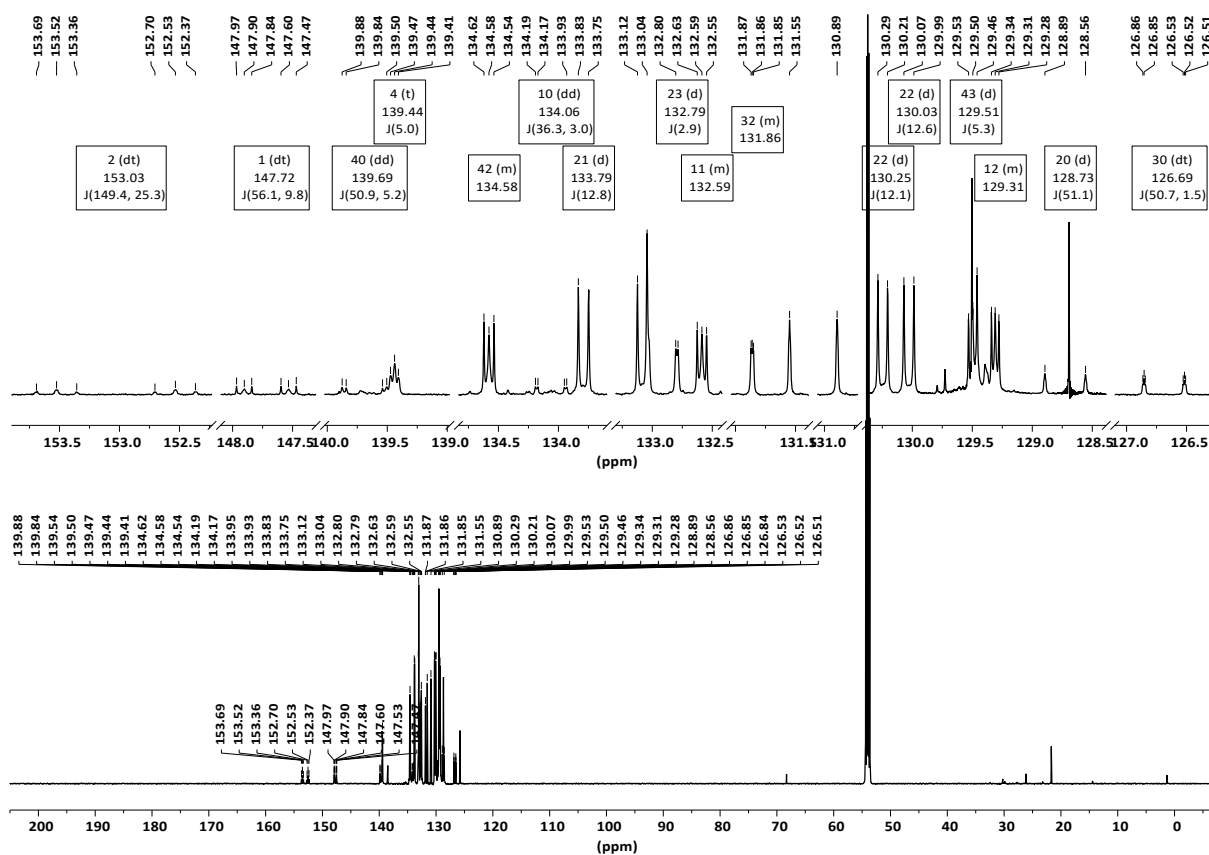
Figure S3b: $^{13}C\{^1H\}$ NMR spectrum (CD$_2$Cl$_2$, 151 MHz) of **2Pd**.
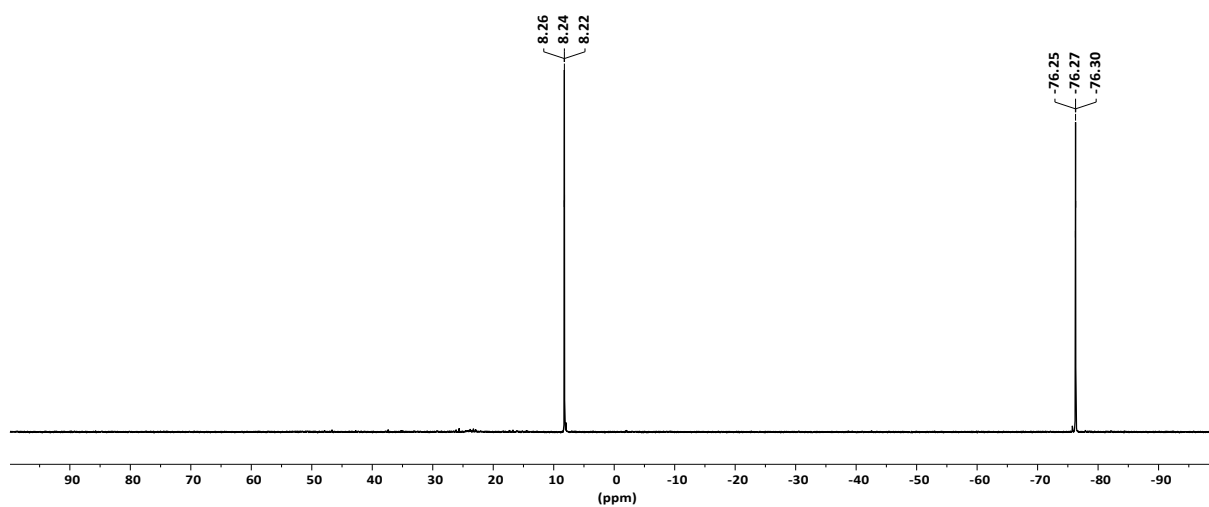
Figure S3c: ^{31}P NMR spectrum (CD$_2$Cl$_2$, 243 MHz) of **2Pd**.
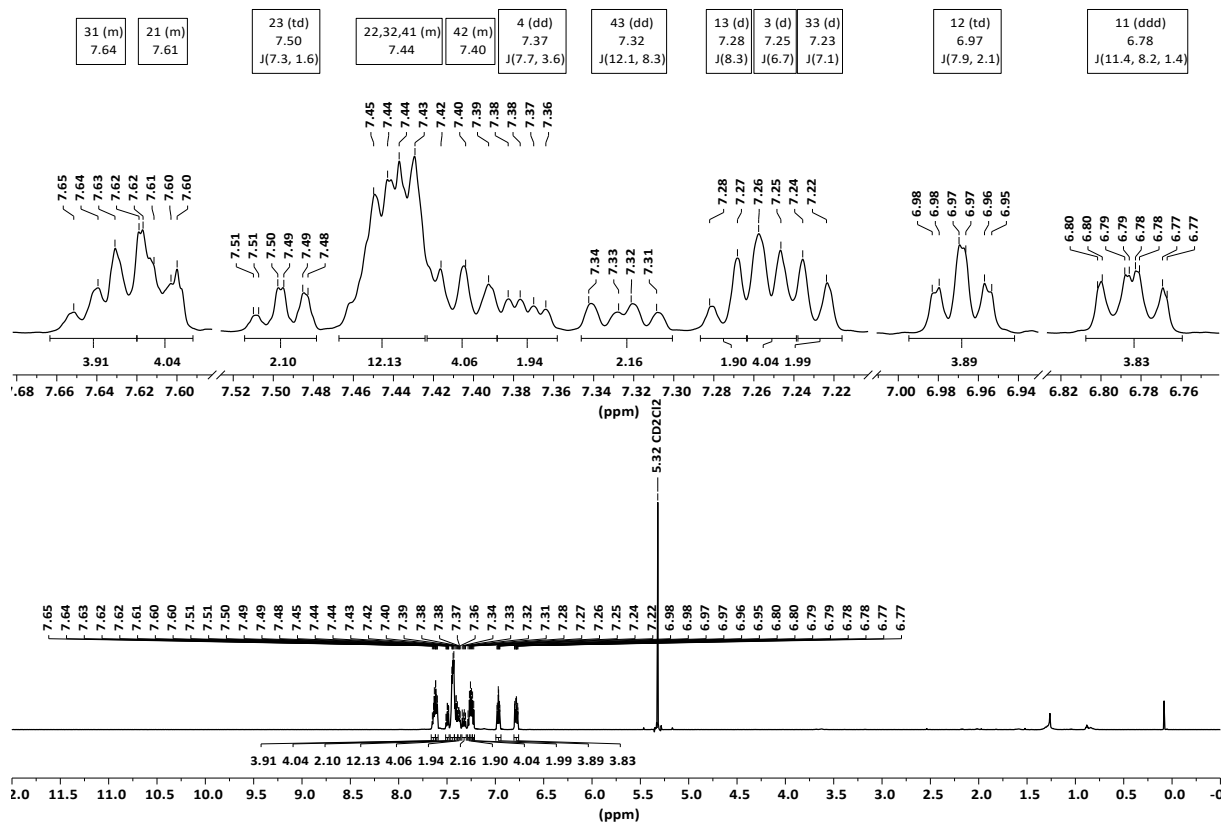
Figure S4a: ¹H NMR spectrum (CD₂Cl₂. 600 MHz) of **2Pt**.
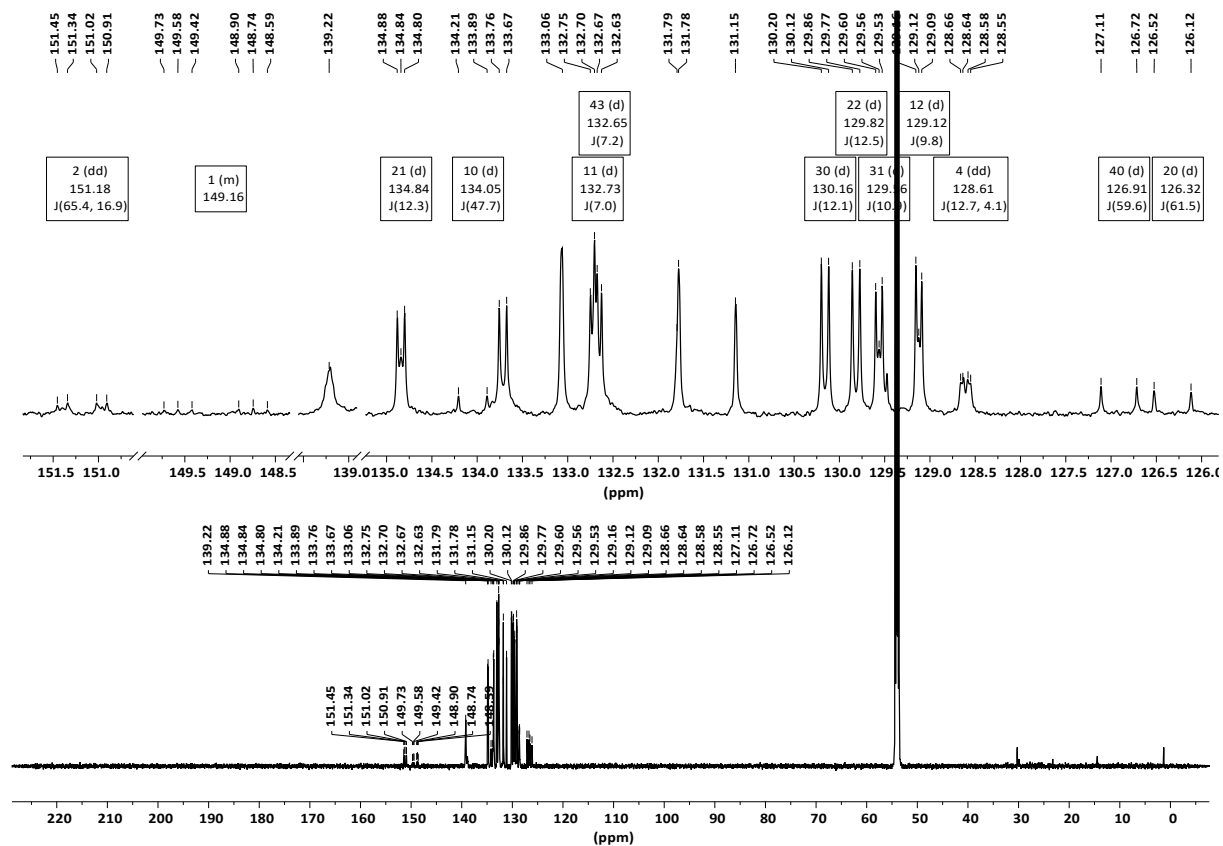
Figure S4b: ¹³C{¹H} NMR spectrum (CD₂Cl₂, 151 MHz) of **2Pt**.

14
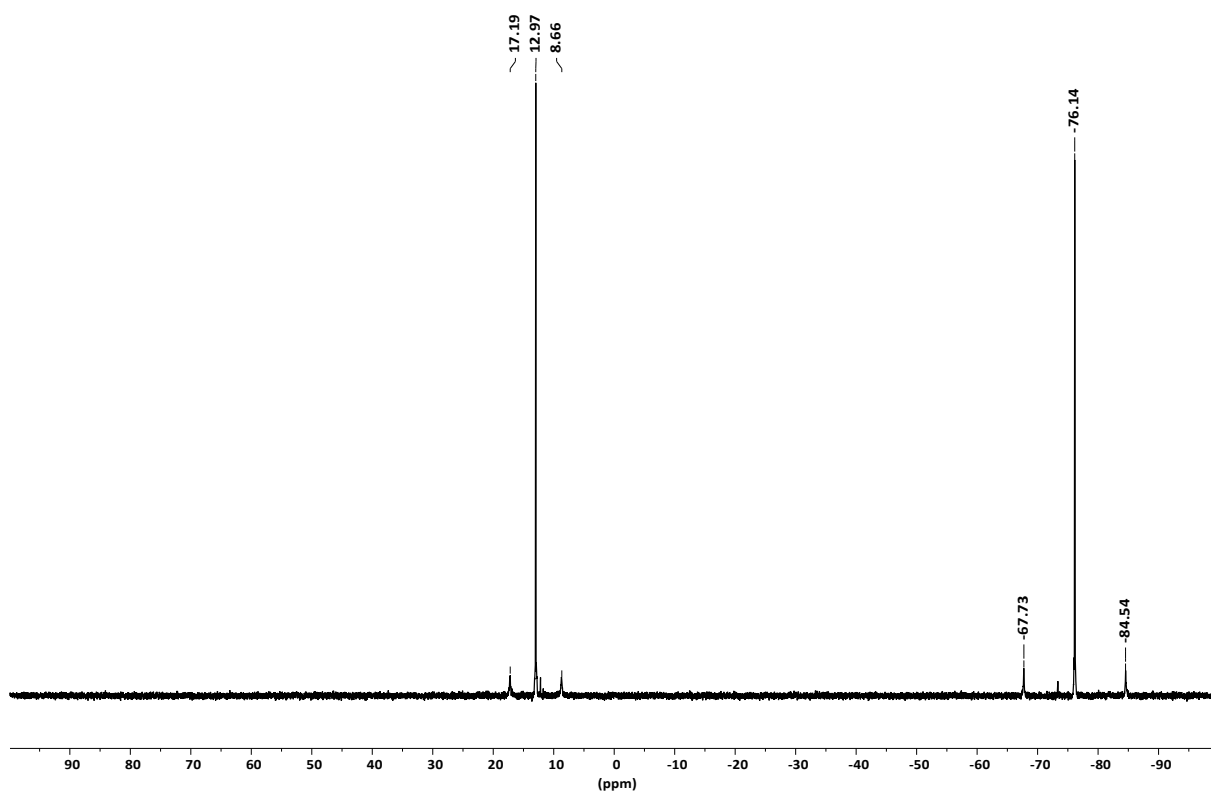
Figure S4c: ^{31}P NMR spectrum (CD$_2$Cl$_2$, 243 MHz) of **2Pt**.

A (dd)	B (d)	C (td)	D (m)	E (m)	F (t)	G (td)	H (dd)	I (t)	J (t)	K (s)
8.06	7.60	7.52	7.36	7.17	7.12	7.04	6.90	6.78	6.21	6.11
J(11.7, 7.5)	J(7.7)	J(8.2, 2.9)			J(7.9)	J(7.3, 2.3)	J(12.4, 7.9)	J(7.5)	J(7.9)	
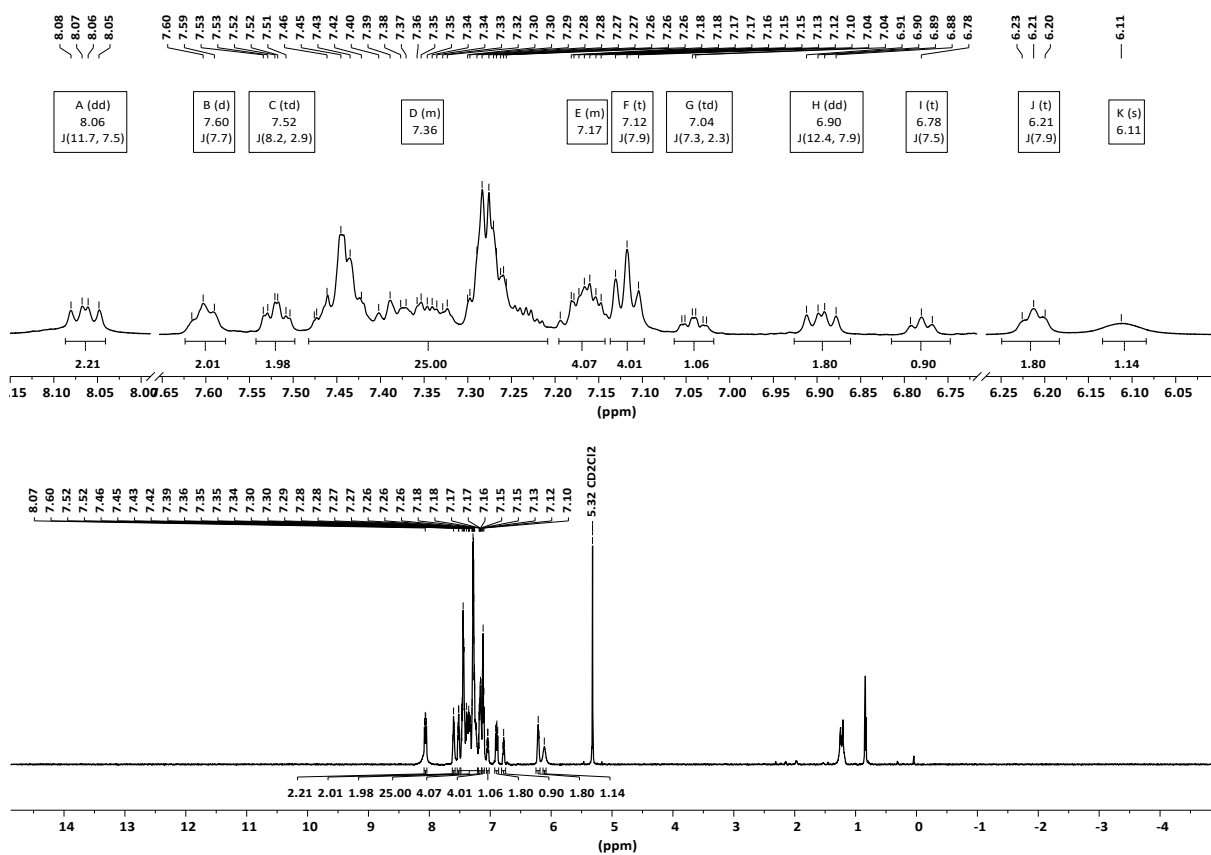
Figure S5a: ^1H NMR spectrum (CD$_2$Cl$_2$. 600 MHz, 243 K) of **1·PtCl$_2$**.
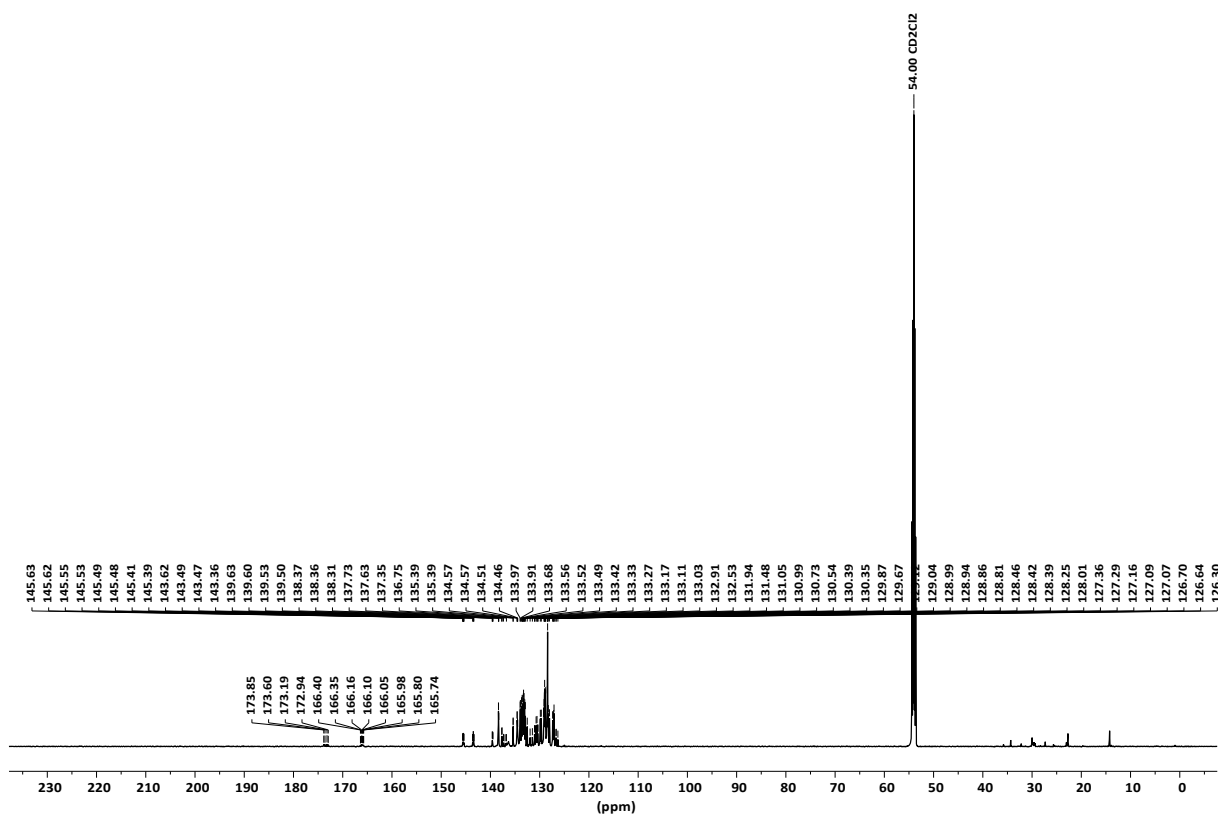
Figure S5b: $^{13}C\{^{1}H\}$ NMR spectrum (CD$_2$Cl$_2$, 151 MHz, 243 K) of **1**·PtCl$_2$.
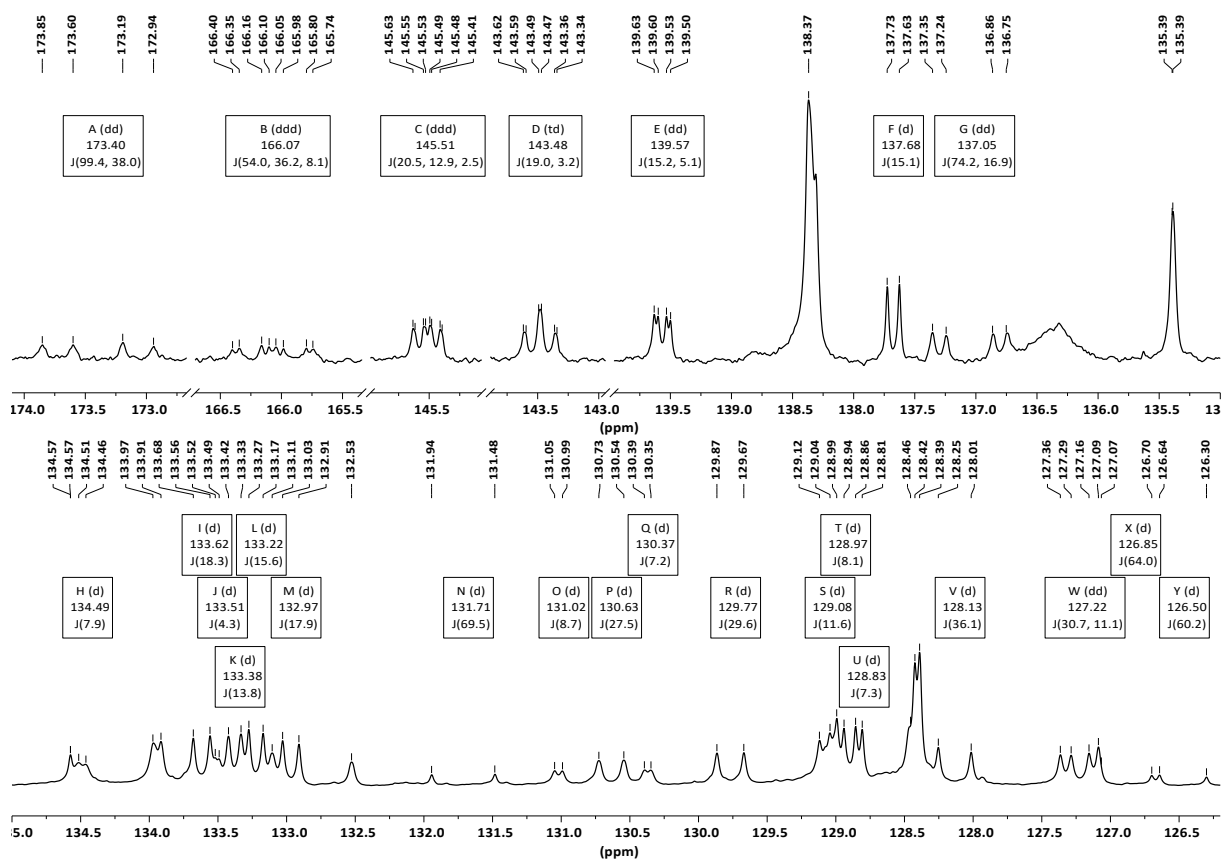
Figure S5c: Detailled $^{13}C\{^{1}H\}$ NMR spectrum (CD$_2$Cl$_2$, 151 MHz, 243 K) of **1**·PtCl$_2$.
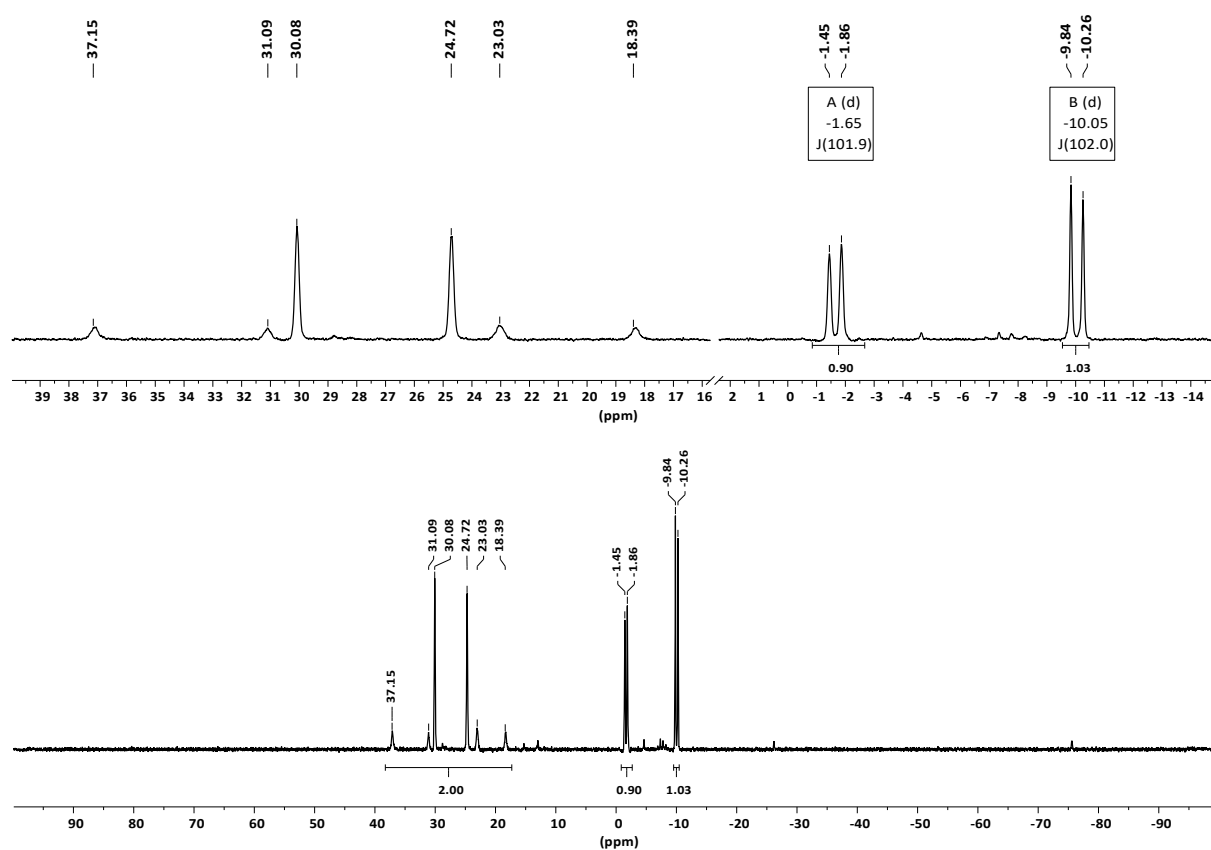
Figure S5d: $^{31}P\{^1H\}$ NMR spectrum (CD$_2$Cl$_2$, 243 MHz, 243 K) of **1·PtCl$_2$**.
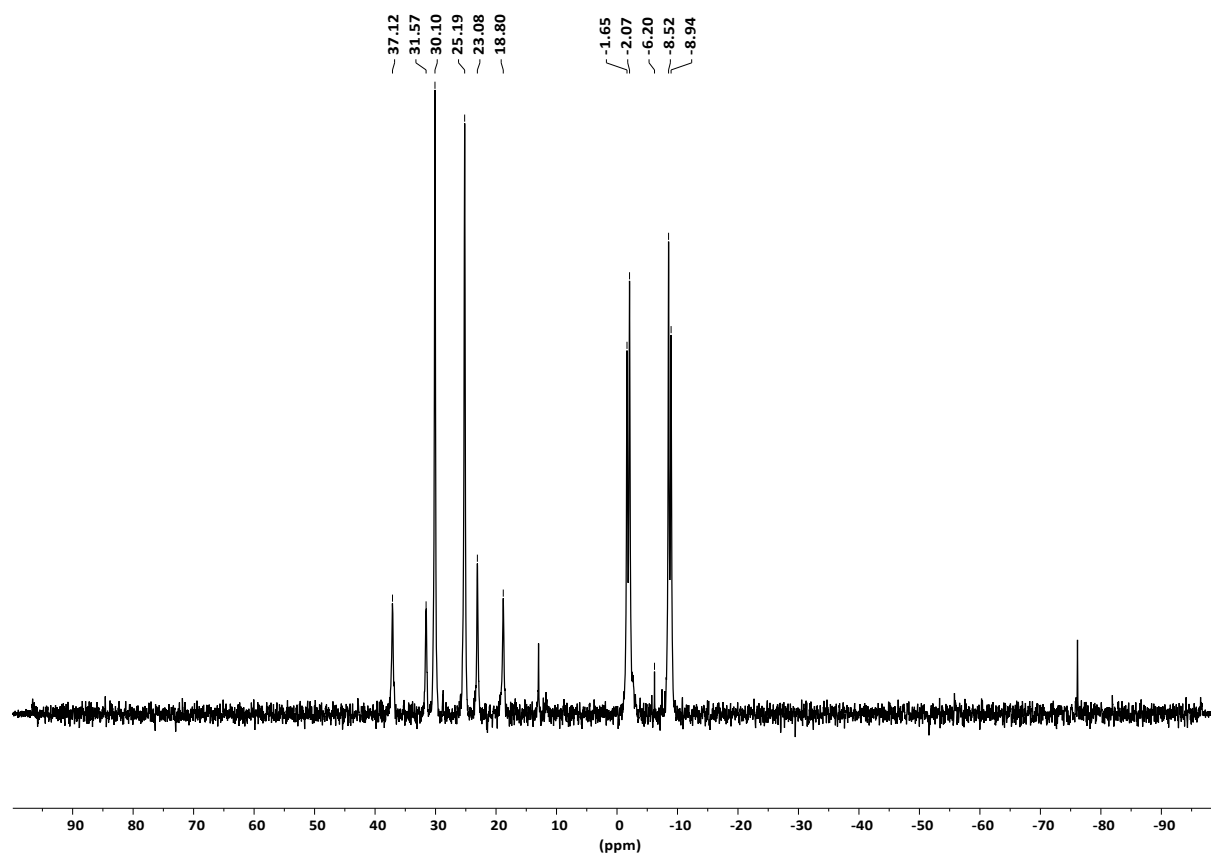
Figure S5e: $^{31}P\{^1H\}$ NMR spectrum (CD$_2$Cl$_2$, 243 MHz, 297 K) of **1·PtCl$_2$**.

UV-vis Spectra
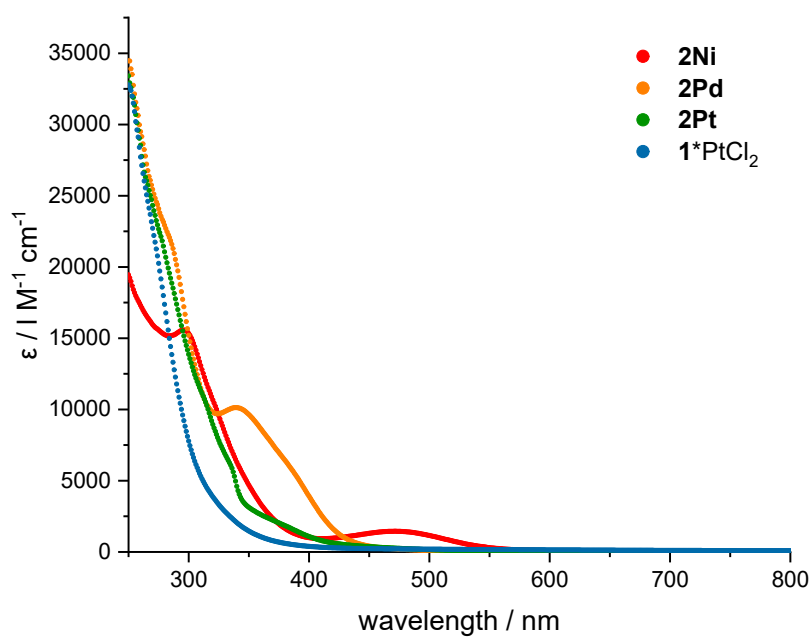
Figure S6a: UV/Vis spectrum of **2Ni** (red), **2Pd** (orange), **2Pt** (green) and **1**·PtCl$_2$ (cyan) in CH$_2$Cl$_2$ as a direct comparison.
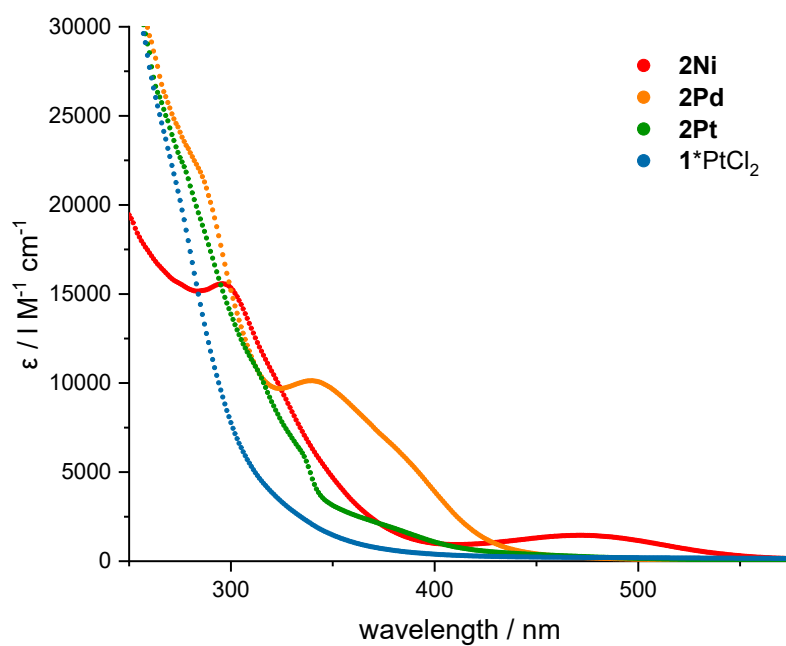
Figure S6b: UV/Vis spectrum (zoom in) of **2Ni** (red), **2Pd** (orange), **2Pt** (green) and **1**·PtCl$_2$ (cyan) in CH$_2$Cl$_2$ as a direct comparison.
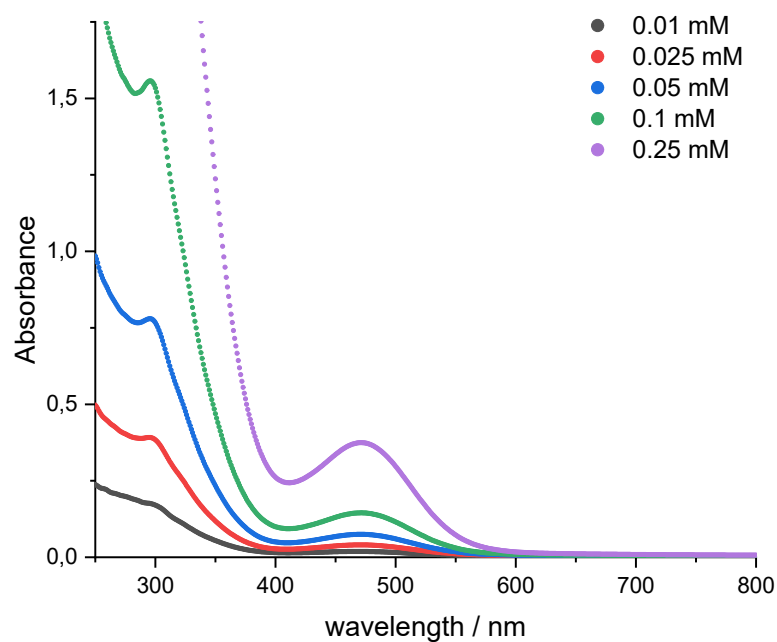
Figure S6c: UV/Vis spectrum of **2Ni** in CH_2Cl_2 for determined concentrations.

Equation	y = a + b*x
Plot	Absorbance
Weight	No Weighting
Intercept	0,00155 ± 0,00227
Slope	1,48399 ± 0,01846
Residual Sum of Squares	3,87381E-5
Pearson's r	0,99977
R-Square (COD)	0,99954
Adj. R-Square	0,99938
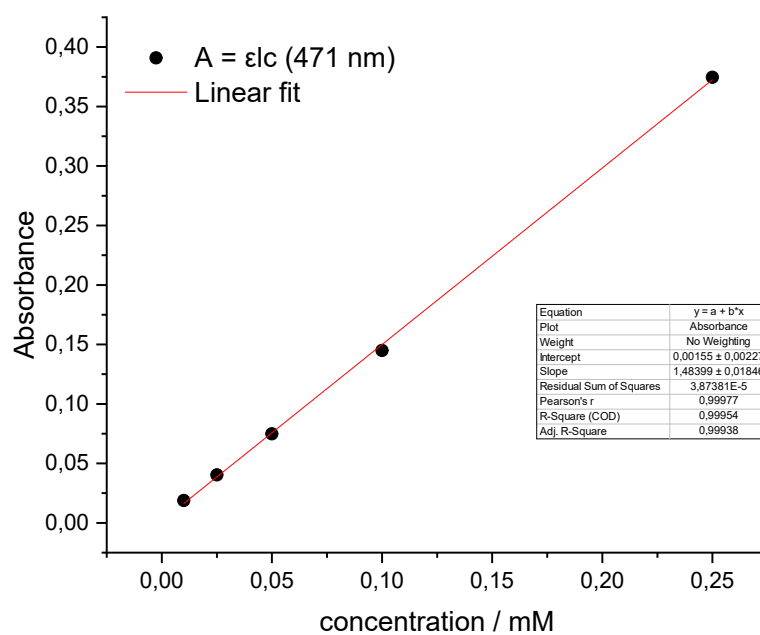
Figure S6d: Concentration–absorbance dependence at 471 nm, absorption maximum of **2Ni** in CH_2Cl_2. Molar absorptivity in the presented range (ε_{471} = 1.484 cm^{-1} M^{-1}) was determined using the Lambert–Beer law.
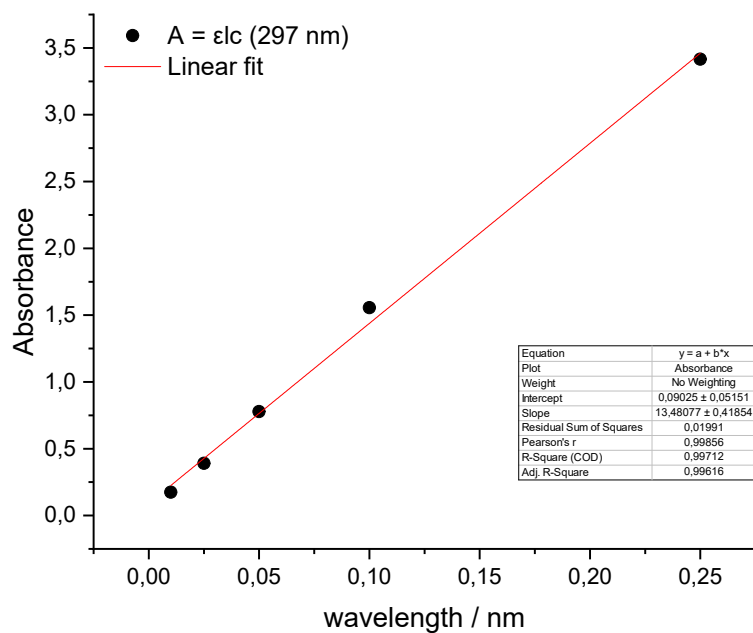
Figure S6e: Concentration–absorbance dependence at 297 nm, absorption maximum of **2Ni** in CH_2Cl_2. Molar absorptivity in the presented range (ε_{297}= 13.481 cm^{-1} M^{-1}) was determined using the Lambert–Beer law.

Figure S6f: UV/Vis spectrum of **2Pd** in CH_2Cl_2 for determined concentrations.

Equation	y = a + b*x
Plot	Absorbance
Weight	No Weighting
Intercept	0,02222 ± 0,00844
Slope	9,90917 ± 0,06861
Residual Sum of Squares	5,34884E-4
Pearson's r	0,99993
R-Square (COD)	0,99986
Adj. R-Square	0,99981

Figure S6g: Concentration–absorbance dependence at 340 nm, absorption maximum of **2Pd** in CH_2Cl_2. Molar absorptivity in the presented range ($\varepsilon_{340} = 9.909$ cm^{-1} M^{-1}) was determined using the Lambert–Beer law.

Figure S6h: UV/Vis spectrum of **2Pt** in CH_2Cl_2 for determined concentrations.
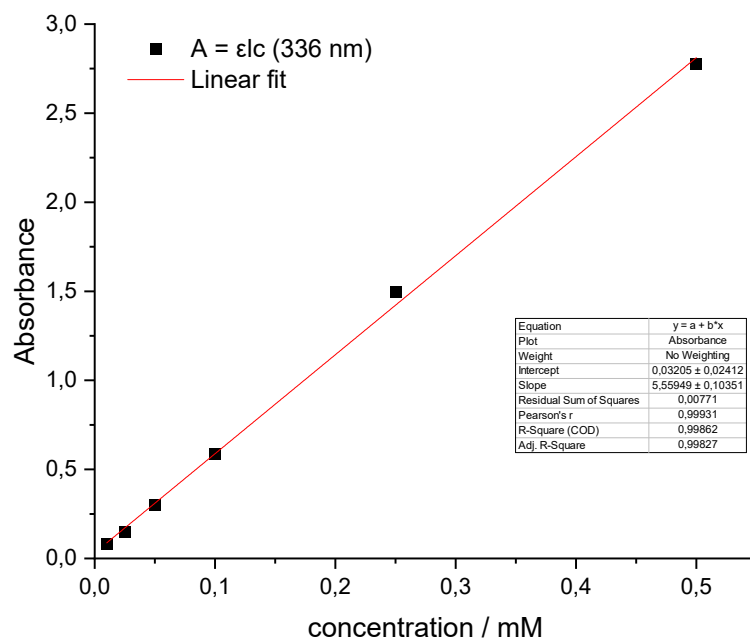
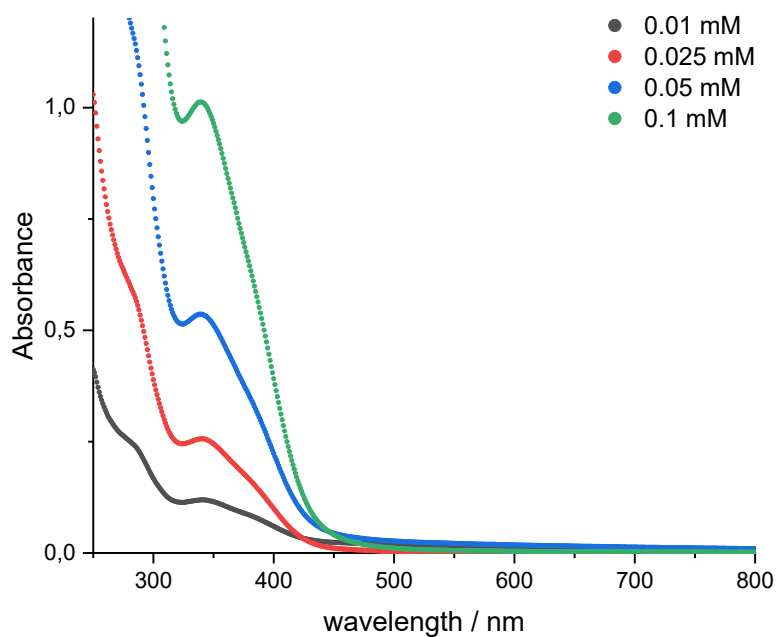**Figure S6i**: Concentration–absorbance dependence at 336 nm, absorption maximum of **2Pt** in CH$_2$Cl$_2$. Molar absorptivity in the presented range (ε_{336} = 5.559 cm^{-1} M^{-1}) was determined using the Lambert–Beer law.
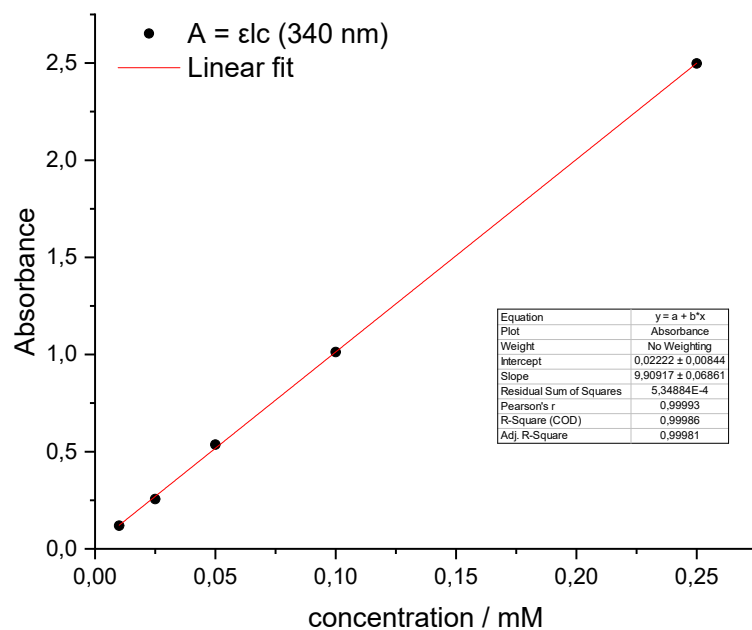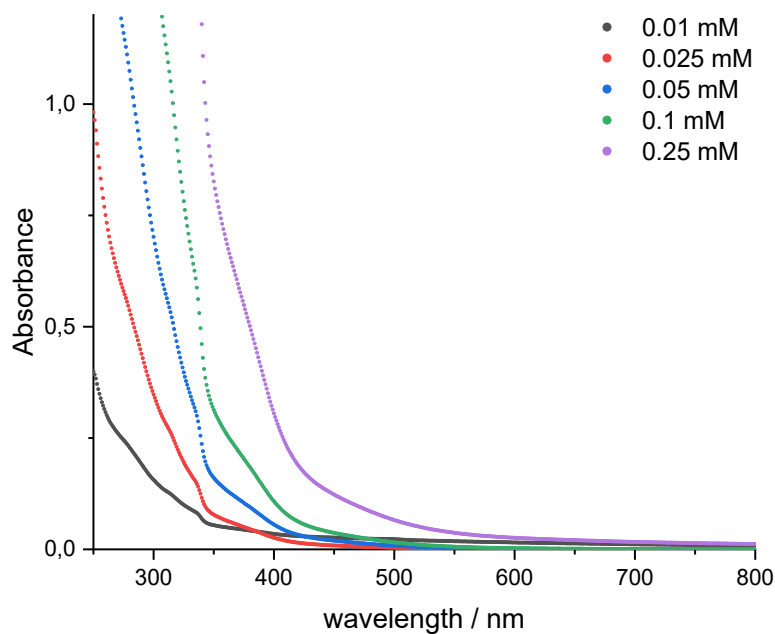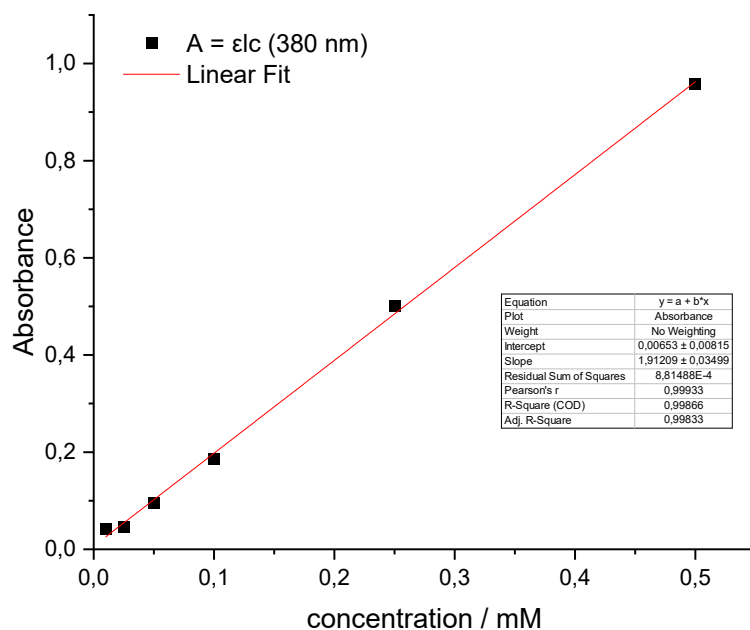

Figure S6j: Concentration–absorbance dependence at 380 nm, absorption maximum of **2Pt** in CH$_2$Cl$_2$. Molar absorptivity in the presented range (ε_{380} = 8.815 cm^{-1} M^{-1}) was determined using the Lambert–Beer law.
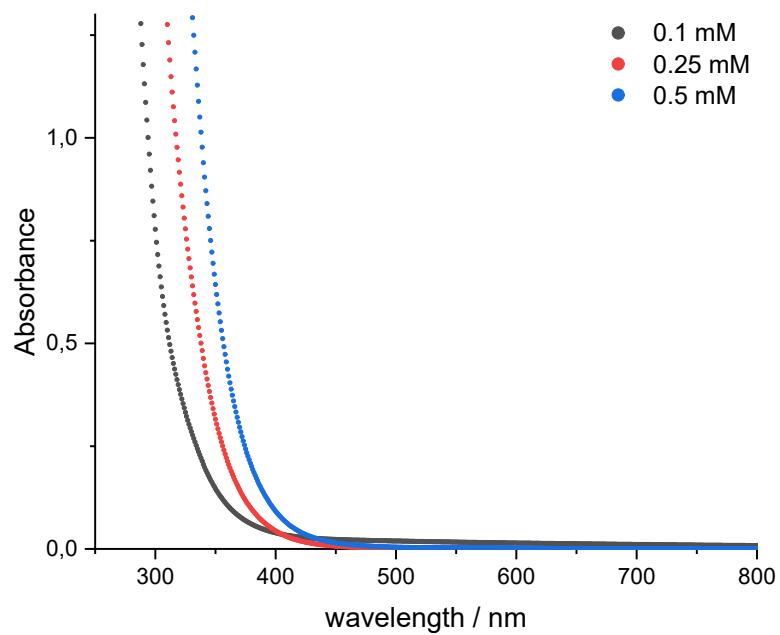
Figure S6k: UV/Vis spectrum of **1**·PtCl$_2$ in CH$_2$Cl$_2$ for determined concentrations.

NMR Spectra of Dehydrogenation of Me₂NHBH₃
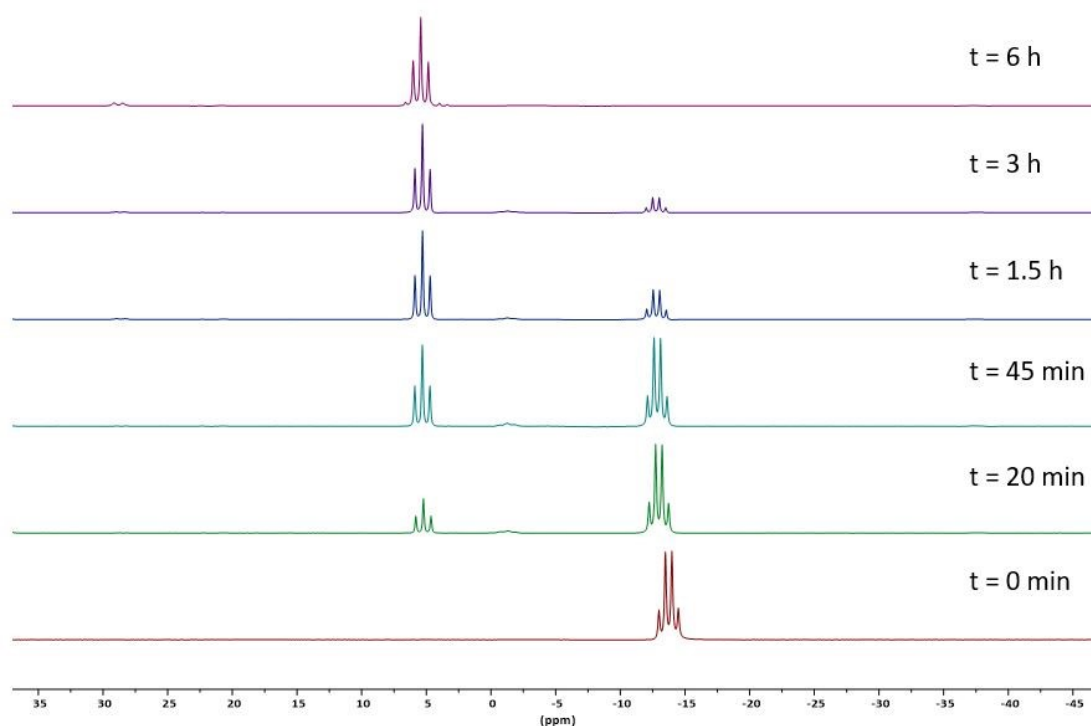
Figure S7a: Stacked plot of ^{11}B NMR spectra (1,2-DFB, 192 MHz, 297.15 K) of the dehydrogenation of Me₂NHBH₃ in the presence of **2Ni** after different reaction times at 343.15 K.
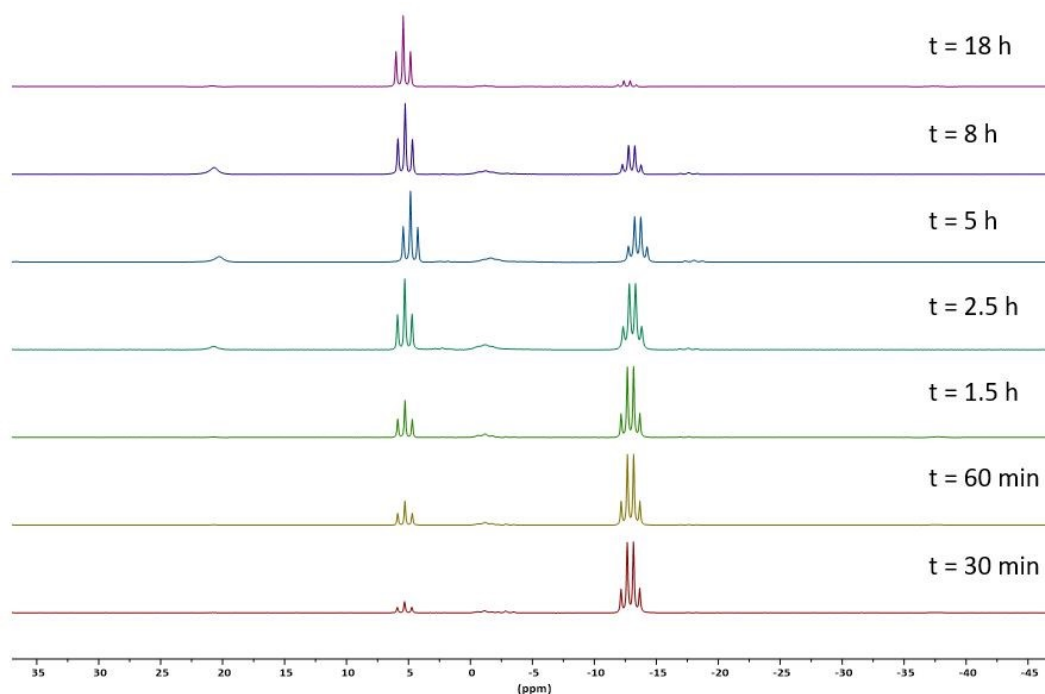
Figure S7b: Stacked plot of ^{11}B NMR spectra (1,2-DFB, 192 MHz, 297.15 K) of the dehydrogenation of Me₂NHBH₃ in the presence of **2Pt** after different reaction times at 343.15 K.
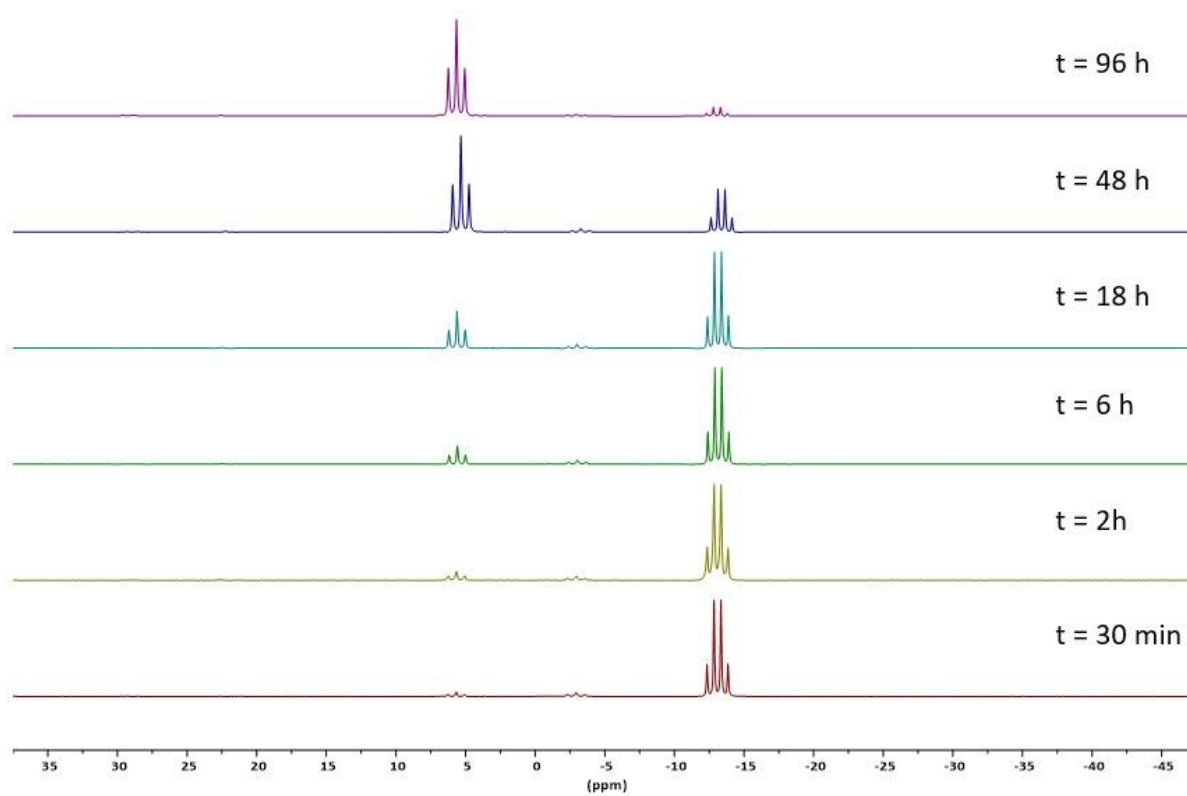
Figure S7c: Stacked plot of ^{11}B NMR spectra (1,2-DFB, 192 MHz, 297.15 K) of the dehydrogenation of Me_2NHBH_3 in the presence of **1**·$PtCl_2$ after different reaction times at 343.15 K.

Crystal and Refinement Data

Intensity data of **1**, **1**·PtCl$_2$, **2Ni**, **2Pd** and **2Pt** were collected at 100 K on a Bruker Venture D8 diffractometer with graphite-monochromated Mo-Kα (0.7107 Å) radiation. All structures were solved by direct methods and refined based on F^2 by use of the SHELX program package as implemented in OLEX 2 version 1.5.[S1] All non-hydrogen atoms were refined using anisotropic displacement parameters. Hydrogen atoms attached to carbon atoms were included in geometrically calculated positions using a riding model. Crystal and refinement data are collected in Table S1. Disorder was resolved for the structures of **1**, **2Pd** and **2Pt**. Residual density plots of **1**, **2Ni**, **2Pd** and **2Pt** are shown in Figures S8a-d. The F$_{obs}$ versus F$_{calc}$ plot of **2Pd** is shown in Figure S9. Figures of the molecular structures were created using DIAMOND.[S2] Crystallographic data for the structural analyses have been deposited with the Cambridge Crystallographic Data Centre. Copies of this information may be obtained free of charge from The Director, CCDC, 12 Union Road, Cambridge CB2 1EZ, UK (Fax: +44-1223-336033; e-mail: deposit@ccdc.cam.ac.uk or http://www.ccdc.cam.ac.

Table S1. Crystal data and structure refinement of **1**, **1**·PtCl$_2$, **2Ni**, **2Pd** and **2Pt**.

	1	**1**·PtCl$_2$·CH$_2$Cl$_2$
Formula	C$_{60}$H$_{46}$ClGaP$_4$	C$_{61}$H$_{48}$Cl$_5$GaP$_4$Pt
Formula weight, g mol^{-1}	996.02	1346.93
Crystal system	Monoclinic	Triclinic
Crystal size, mm	0.30 × 0.20 × 0.10	0.20 × 0.15 × 0.10
Space group	P2$_1$/c	P$\bar{1}$
a, Å	25.641(2)	10.9998(12)
b, Å	10.5252(9)	12.2209(13)
c, Å	19.2556(15)	21.688(2)
α, °	90	89.922(4)
β, °	109.104(4)	83.531(4)
γ, °	90	69.049(4)
V, Å^3	4910.4(7)	2703.0(5)
Z	4	2
ρ_{calcd}, Mg m^{-3}	1.347	1.655
μ (Mo $K\alpha$), mm^{-1}	0.785	3.490
$F(000)$	2056	1336
θ range, deg	2.11 to 28.28	2.15 to 30.51
Index ranges	−34 ≤ h ≤ 34	−15 ≤ h ≤ 15
	−14 ≤ k ≤ 14	−17 ≤ k ≤ 17
	−25 ≤ l ≤ 25	−30 ≤ l ≤ 30
No. of reflns collected	151264	111439
Completeness to θ_{max}	99.9%	99.9%
No. indep. Reflns	12167	16386
No. obsd reflns with ($I>2\sigma(I)$)	10186	15329
No. refined params	613	649
GooF (F^2)	1.076	1.066
R_1 (F) ($I > 2\sigma(I)$)	0.0405	0.0285
wR_2 (F^2) (all data)	0.0952	0.0639
Largest diff peak/hole, e Å^{-3}	0.884 / −0.553	1.773 / −1.056
CCDC number	2378087	2378088

Table S1.   Cont.

2Ni	2Pd	2Pt
$C_{60}H_{46}Cl_5GaNi_2P_4$	$C_{60}H_{46}Cl_5GaP_4Pd_2$	$C_{60}H_{46}Cl_5GaP_4Pt_2$
1255.24	1350.62	1528.00
Triclinic	Triclinic	Triclinic
$0.30 \times 0.25 \times 0.20$	$0.21 \times 0.17 \times 0.16$	$0.50 \times 0.50 \times 0.40$
$P\bar{1}$	$P\bar{1}$	$P\bar{1}$
14.839(3)	15.1433(6)	13.4598(4)
15.097(2)	15.3082(5)	15.8581(4)
15.823(3)	15.6366(6)	16.9458(5)
100.633(5)	77.139(2)	70.1200(10)
98.985(6)	61.775(2)	86.2630(10)
111.337(5)	89.651(2)	89.4130(10)
3146.9(8)	3092.9(2)	3393.97(17)
2	2	2
1.325	1.450	4.829
1.366	1.362	1.495
1276	1348	9653
2.07 to 27.51	2.64 to 25.06	2.10 to 26.37
$-21 \leq h \leq 21$	$-18 \leq h \leq 18$	$-16 \leq h \leq 16$
$-21 \leq k \leq 17$	$-18 \leq k \leq 18$	$-19 \leq k \leq 19$
$-22 \leq l \leq 22$	$-18 \leq l \leq 18$	$-21 \leq l \leq 21$
54603	71038	86562
99.8%	99.8%	99.7%
19289	10960	13819
13370	9678	12885
667	757	649
1.028	1.191	1.068
0.0373	0.0693	0.0239
0.0879	0.1870	0.0605
0.609 / −0.509	1.570 / −0.996	1.483 / −0.894
2378089	2378090	2378091
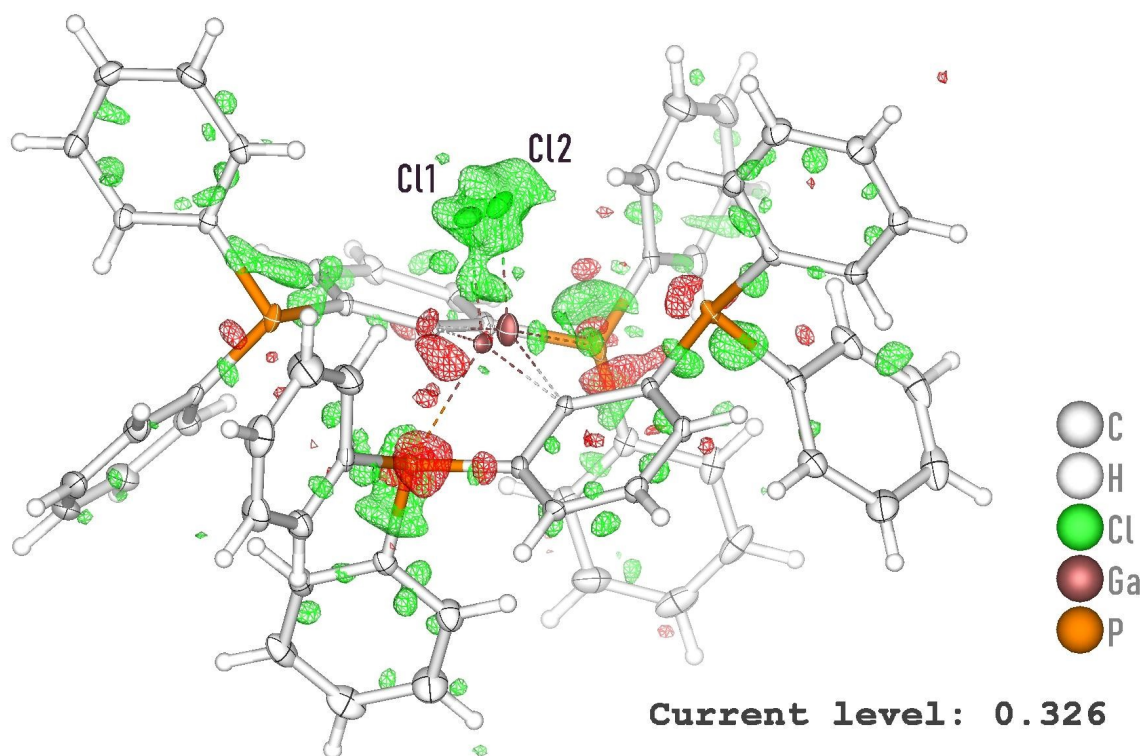
Figure S8a: Residual density plot of **1**.
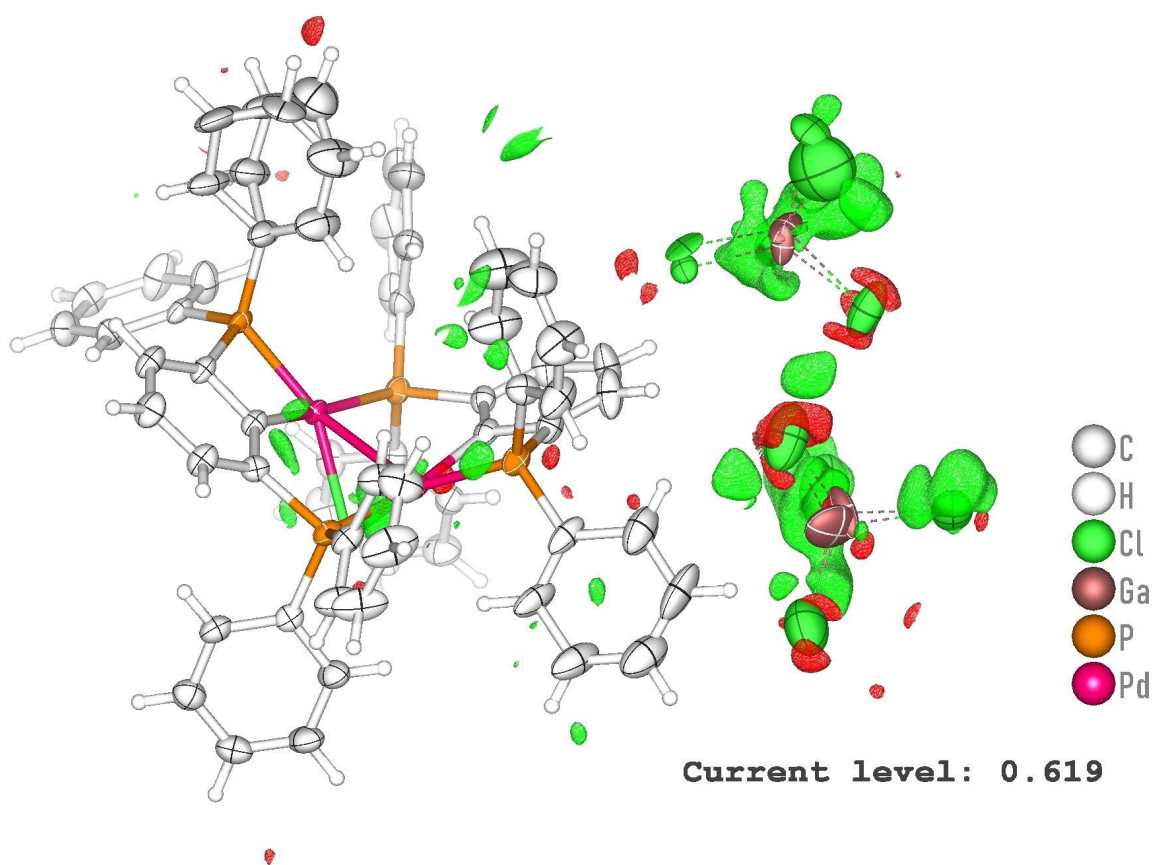
Figure S8b: Residual density plot of **2Ni**.

Current level: 0.362
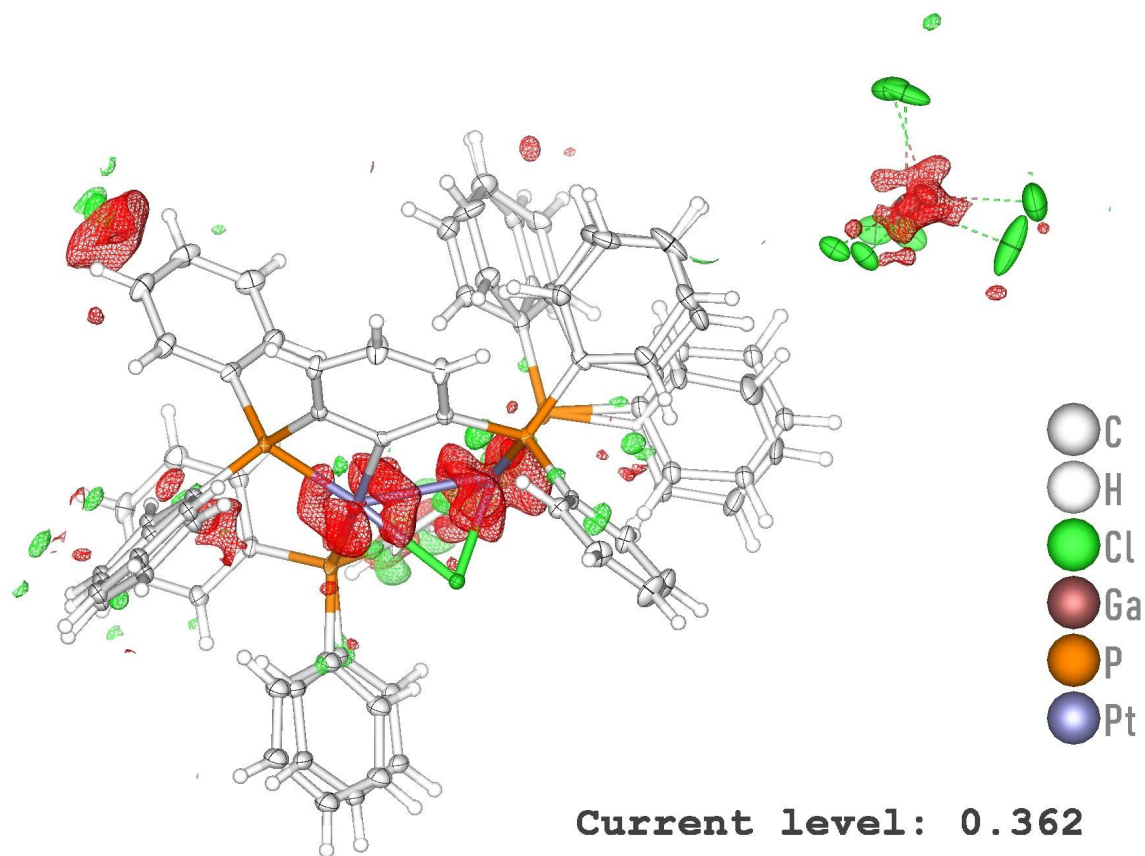
Figure S8c: Residual density plot of **2Pd**.

Current level: 0.348
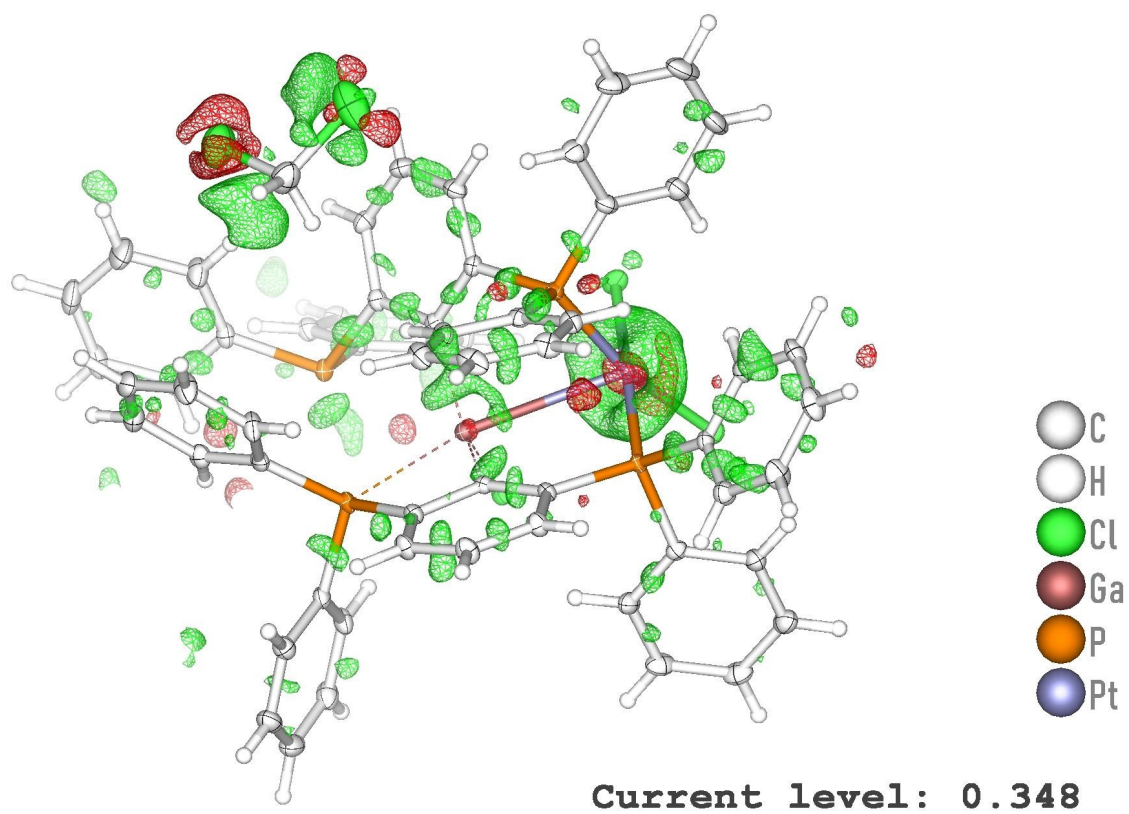
Figure S8d: Residual density plot of **2Pt**.
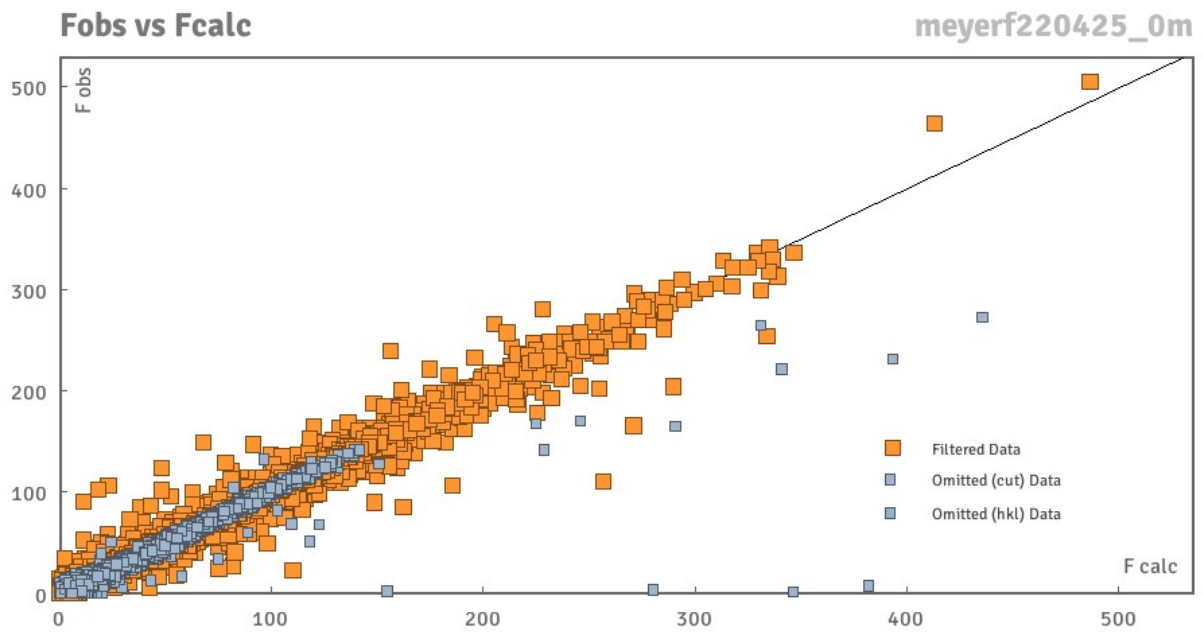
Figure S9: F_{obs} versus F_{calc} plot of **2Pd**.

DFT Computations

Computational Methodology

Geometry optimizations of the isolated molecular structures were carried out using density functional theory (DFT) at the B3PW91/6-311+G(2df,p)[S3,S4] level of theory using the Gaussian16[S5] software package. For the Ni (ECP10MDF), Pd (ECP28MDF) and Pt (ECP60MDF) atoms, effective core potentials and corresponding cc-pVTZ basis sets were used.[S6] Dispersion effects were modelled using Grimme's GD3BJ parameters.[S7] Wavefunction files were used for a topological analysis of the electron density according to the Atoms-In-Molecules partitioning scheme[11] using AIMAll,[S8] The NCI[12] grids were computed with NCIplot.[S9] Independent gradient model based on Hirshfeld partition (IGMH)[13] analysis were obtained with Multiwfn_3.8.[S10] AIM, IGMH and NCI figures are displayed using Multiwfn 3.8[S10] and VMD.[S11] Both, the NCI as well as the IGMH approach are capable of visualizing weak non-covalent interactions. Within the IGMH approach individual fragments can be defined and the inter- and intramolecular interactions can be visualized separately, which is an advantage for large and crowded systems such as studied here.

Table S2. Topological and integrated bond properties from AIM of **2Ni**, **2Pd** and **2Pt**.

| Species	d [Å]	$\rho(r)$ [eÅ^{-3}]	$\nabla^2\rho(r)$ [eÅ^{-5}]	ε	$G/\rho(r)$ [a.u.]	$H/\rho(r)$ [a.u.]	δ	q_{AIM} [e]
2Ni								
Ni-Ni		0.22*	1.1*				0.17	Ni1: 0.51
Ni1-Cl	2.222	0.50	6.9	0.11	1.12	–0.15	0.59	Ni2: 0.51
Ni2-Cl	2.222	0.50	6.9	0.11	1.12	–0.15	0.59	Cl: -0.55
P4-Ni1	2.221	0.60	4.3	0.04	0.78	–0.27	0.69	P4: 1.66
P5-Ni1	2.135	0.72	3.8	0.06	0.70	–0.33	0.82	P5: 1.79
P6-Ni2	2.221	0.60	4.3	0.04	0.78	–0.27	0.69	P6: 1.66
P7-Ni2	2.135	0.72	3.8	0.06	0.70	–0.33	0.82	P7: 1.79
2Pd								
Pd-Pd	2.773	0.26	2.4	0.25	0.80	–0.16	0.26	Pd1: 0.19
Pd1-Cl3	2.401	0.49	4.8	0.08	0.95	–0.25	0.62	Pd2: 0.19
Pd2-Cl3	2.401	0.49	4.8	0.08	0.95	–0.25	0.62	Cl3: -0.49
P4-Pd1	2.335	0.64	2.8	0.04	0.69	–0.38	0.78	P4: 1.72
P5-Pd1	2.228	0.79	1.4	0.08	0.60	–0.48	0.90	P5: 1.90
P6-Pd2	2.335	0.64	2.8	0.04	0.69	–0.38	0.78	P6: 1.72
P7-Pd2	2.228	0.79	1.4	0.08	0.60	–0.48	0.90	P7: 1.90
2Pt								
Pt-Pt	2.811	0.32	2.5	0.09	0.74	–0.21	0.37	Pt1: 0.05
Pt1-Cl3	2.419	0.53	4.6	0.09	0.89	–0.29	0.69	Pt2: 0.05
Pt2-Cl3	2.419	0.53	4.6	0.09	0.89	–0.29	0.69	Cl3: -0.44
P4-Pt1	2.324	0.74	2.2	0.04	0.65	–0.44	0.90	P4: 1.76
P5-Pt1	2.217	0.91	–0.1	0.10	0.54	–0.55	1.01	P5: 1.96
P6-Pt2	2.324	0.74	2.2	0.04	0.65	–0.44	0.90	P6: 1.76
P7-Pt2	2.217	0.91	–0.1	0.10	0.54	–0.55	1.01	P7: 1.96

* Values are derived from inspection of the properties along the Ni-Ni line, no bcp were observed.
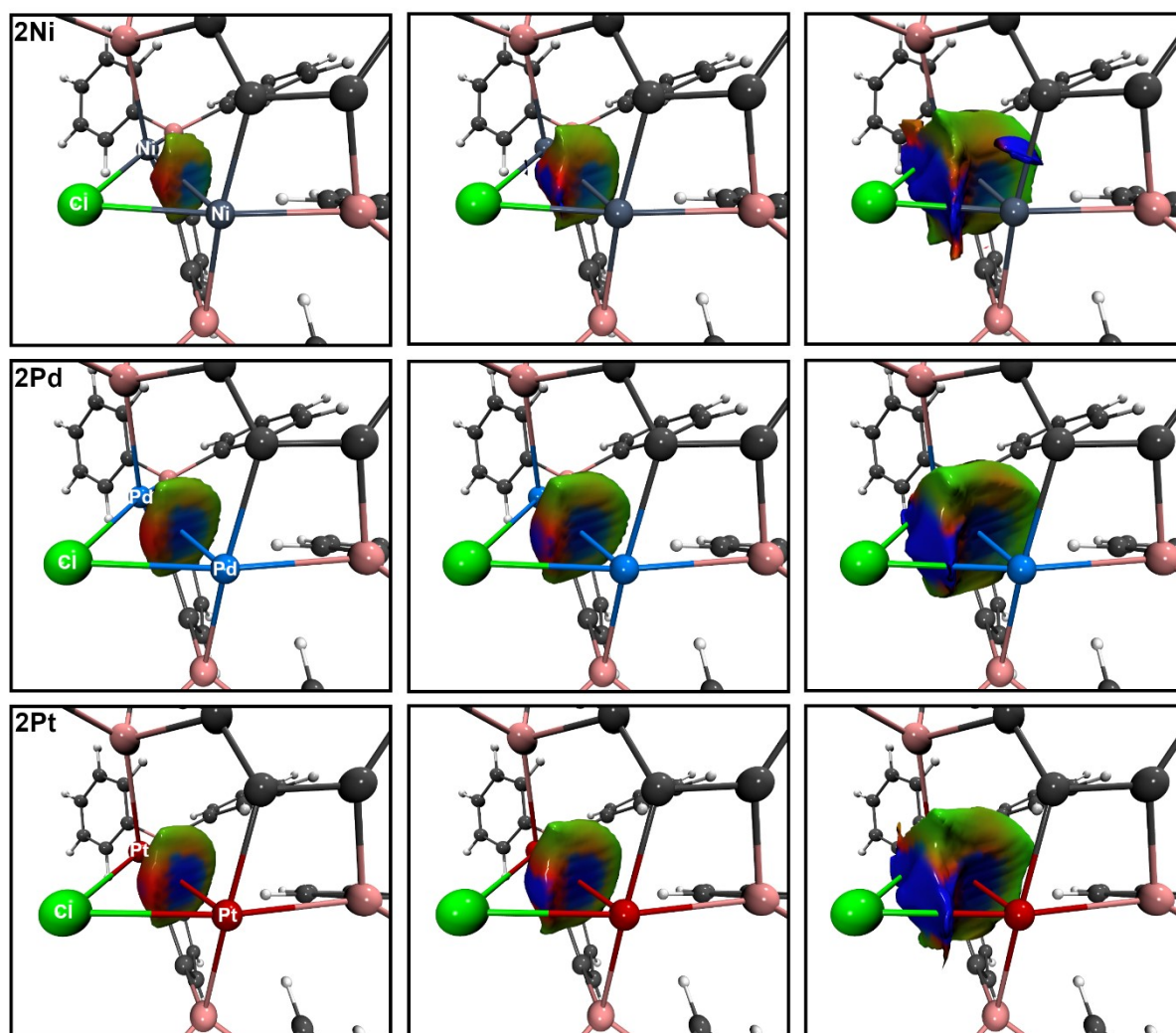
Figure S10: IGM based on a Hirshfeld partition of the molecular density of **2M** (B3PW91/6-311+G(2df,p)). Each metal atom defines one fragment. IGMH iso-surfaces at s(r) = 0.010 (left), s(r) = 0.005 (middle) and s(r) = 0.001 (right) colour coded with sign(λ2)ρ in a. u. Blue surfaces refer to attractive forces and red to repulsive forces. Green indicates weak interactions
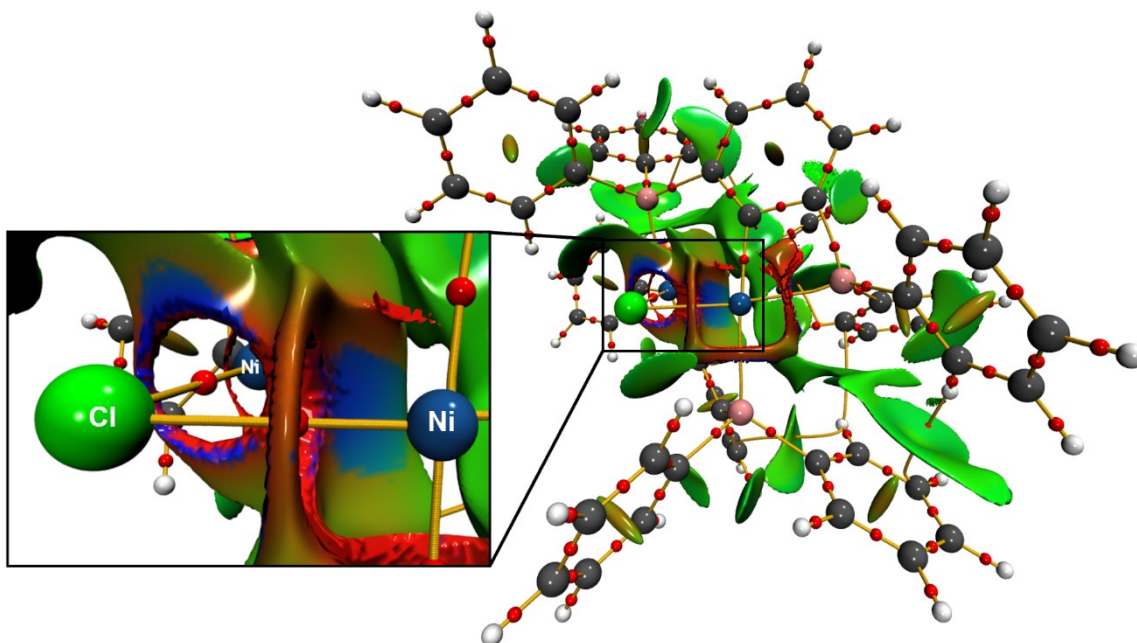
Figure S11: AIM molecular graph of **2Ni** (B3PW91/6-311+G(2df,p)) with bond critical points as red spheres and bond paths in orange as well as NCI iso-surfaces at s(r) = 0.5 colour coded with sign(λ2)ρ in a. u. Blue surfaces refer to attractive forces and red to repulsive forces. Green indicates weak interactions.
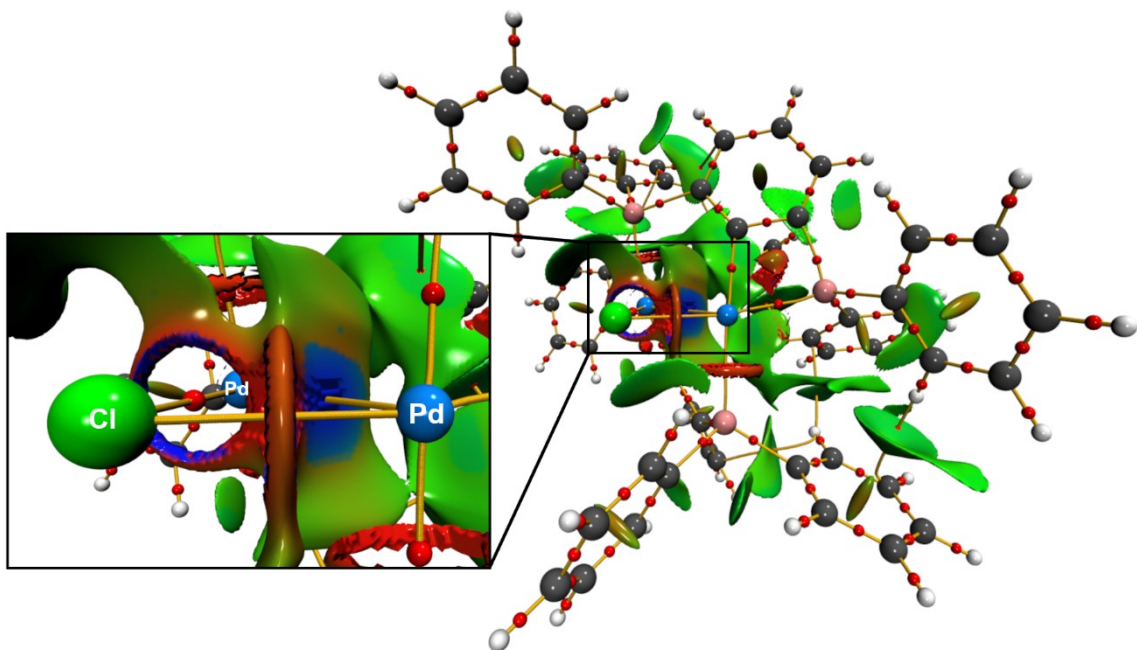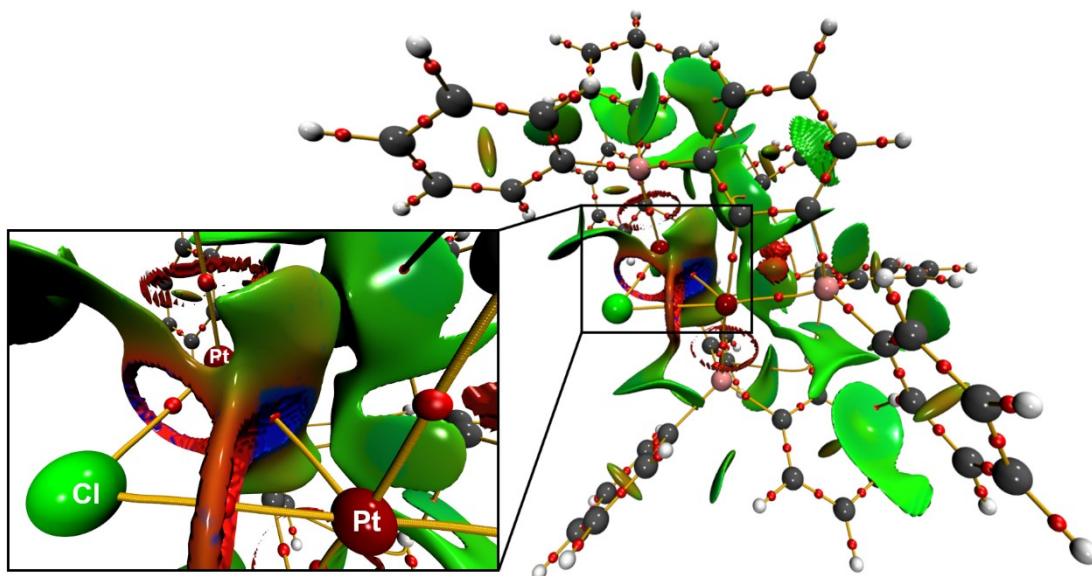

Figure S12: AIM molecular graph of **2Pd** (B3PW91/6-311+G(2df,p)) with bond critical points as red spheres and bond paths in orange as well as NCI iso-surfaces at s(r) = 0.5 colour coded with sign(λ2)ρ in a. u. Blue surfaces refer to attractive forces and red to repulsive forces. Green indicates weak interactions.

Figure S13: AIM molecular graph of **2Pt** (B3PW91/6-311+G(2df,p)) with bond critical points as red spheres and bond paths in orange as well as NCI iso-surfaces at s(r) = 0.5 colour coded with sign(λ2)ρ in a. u. Blue surfaces refer to attractive forces and red to repulsive forces. Green indicates weak interactions.

Additional References

[S1]   O. V. Dolomanov, L. J. Bourhis, R. J. Gildea, J. A. K. Howard, H. Puschmann, *J. Appl. Cryst.* 2009, **42**, 339-341.

[S2]   K. Brandenburg DIAMOND version 3.2i, Crystal Impact GbR, Bonn Germany 2012.

[S3]   (a) A. D. Becke *J. Chem. Phys.* 1993, **98**, 5648-5652. (b) J. P. Perdew , J. A. Chevary , S. H. Vosko , K. A. Jackson , M. R. Pederson , D. J. Singh and C. Fiolhais, *Phys. Rev. B: Condens. Matter Mater. Phys.* 1992, **46**, 6671-6687.

[S4]   (a) R. Krishnan, J. S. Binkley, R. Seeger and J. A. Pople, *J. Chem. Phys.* 1980, **72**, 650-654. (b) A. D. McLean and G. S. Chandler, *J. Chem. Phys.* 1980, **72**, 5639-5648.

[S5]   M. J. Frisch, G. W. Trucks, H. B. Schlegel, G. E. Scuseria, M. A. Robb, J. R. Cheeseman, G. Scalmani, V. Barone, G. A. Petersson, H. Nakatsuji, X. Li, M. Caricato, A. V.Marenich, J. Bloino, B. G. Janesko, R. Gomperts, B. Mennucci, H. P. Hratchian, J. V. Ortiz, A. F. Izmaylov, J. L. Sonnenberg, D. Williams-Young, F. Ding, F. Lipparini, F. Egidi, J. Goings, B. Peng, A. Petrone, T. Henderson, D. Ranasinghe, V. G. Zakrzewski, J. Gao, N. Rega, G. Zheng, W. Liang, M. Hada, M.Ehara, K.Toyota, R. Fukuda, J. Hasegawa, M. Ishida, T. Nakajima, Y. Honda, O.Kitao, H. Nakai, T. Vreven, K. Throssell, J. A. Montgomery Jr., J. E.Peralta, F. Ogliaro, M. J. Bearpark, J. J. Heyd, E. N. Brothers, K. N. Kudin, V. N.Staroverov, T. A. Keith, R. Kobayashi, J. Normand, K. Raghavachari, A. P. Rendell, J. C. Burant, S. S. Iyengar, J. Tomasi, M. Cossi, J. M. Millam, M. Klene, C. Adamo, R. Cammi, J. W. Ochterski, R. L. Martin, K. Morokuma, O. Farkas, J. B. Foresman and D. J. Fox, Gaussian16 (RevisionC.01), Gaussian, Inc., Wallingford CT, 2019.

[S6]   (a) M. Dolg, U. Wedig, H. Stoll, H. Preuss, J. Chem. Phys. 1987, **86**, 866-872. (b) B. Metz , H. Stoll and M. Dolg, *J. Chem. Phys.* 2000, **113**, 2563-2569. (c) J. M. L. Martin, A. Sundermann, *J. Chem. Phys.* 2001, **114**, 3408-3420. (d) K. A. Petersen, D. Figgen,

M. Dolg, H. Stoll, *J. Chem. Phys.* 2007, **126**, 124101-124112. (e) D. Figgen, K. A. Petersen, M. Dolg, H. Stoll, *J. Chem. Phys.* 2009, **130**, 164108-164120.

[S7]   S. Grimme , S. Ehrlich and L. Goerigk, *J. Comput. Chem.* 2011, **32**, 1456-1465.

[S8]   A. Todd, AIMAll (Version 15.09.27), Keith, TK Gristmill Software, Overland Park KS, USA, 2015 (aim.tkgristmill.com).

[S9]   J. Contreras-García , E. Johnson , S. Keinan , R. Chaudret , J.-P. Piquemal , D. Beratan and W. Yang, *J. Chem. Theory Comput.* 2011, **7**, 625-632.

[S10]   T. Lu and F. Chen , *J. Comput. Chem*., 2012, **33**, 580-592.

[S11]   W. Humphrey , A. Dalke and K. Schulten *J. Mol. Graphics* 1996, **14**, 33-38.